ARTICLES

np scattering measurements at 162 MeV and the πNN coupling constant

J. Rahm, J. Blomgren, H. Condé, S. Dangtip, K. Elmgren, N. Olsson, T. Rönnqvist,* and R. Zorro†
Department of Neutron Research, Uppsala University, Box 535, S-75121 Uppsala, Sweden

A. Ringbom‡ and G. Tibell
Department of Radiation Sciences, Uppsala University, Box 535, S-75121 Uppsala, Sweden

O. Jonsson, L. Nilsson, and P.-U. Renberg
The Svedberg Laboratory, Uppsala University, Box 533, S-75121 Uppsala, Sweden

T. E. O. Ericson
European Organization for Nuclear Research, CH-1211 Geneva 23, Switzerland
and The Svedberg Laboratory, Uppsala University, Box 533, S-75121 Uppsala, Sweden

B. Loiseau
Division de Physique Théorique, Institut de Physique Nucléaire, 91406 Orsay Cedex, France
and LPTPE Université Pierre and Marie Curie, 4 Place Jussieu, 75252 Paris Cedex 05, France
(Received 8 August 1997)

The differential *np* scattering cross section has been measured at 162 MeV in the angular range $\theta_{\text{c.m.}} = 72° - 180°$, using the neutron beam facility at The Svedberg Laboratory in Uppsala. Special attention was paid to the absolute normalization of the data. In the angular range $150° - 180°$, the data are steeper than those of most previous measurements and predictions from energy-dependent partial-wave analyses or nucleon-nucleon potentials. At 180°, the difference is of the order of 10–15%, an important change since this cross section is considered as a primary standard. It has also consequences for fundamental physics. Moreover, a value of the charged πNN coupling constant, $g^2_{\pi^\pm} = 14.52 \pm 0.26$ ($f^2_{\pi^\pm} = 0.0803 \pm 0.0014$), is deduced from the data, using a novel extrapolation method. This is in good agreement with the classical text book value, but higher than those determined in recent partial-wave analyses of the nucleon-nucleon data base. [S0556-2813(98)01703-8]

PACS number(s): 13.75.Cs, 13.75.Gx, 21.30.−x

I. INTRODUCTION

The precise value of the πNN coupling constant is of crucial importance for the quantitative discussion of a large number of phenomena in hadron and nuclear physics, as well as for the predictions by low-energy theorems of pion photoproduction and leptoproduction, for the Goldberger-Treiman relation, etc. Its strength governs the properties of the two-nucleon system to such an extent that only a few percent difference in its value is sufficient to either unbind the deuteron or to produce a bound diproton, in both cases with major consequences for the world as we know it.

Around 1980, it was believed that the πNN coupling constant was well known. Koch and Pietarinen [1] obtained a value of the charged pion coupling constant $g^2_{\pi^\pm} = 14.28 \pm 0.18$ from $\pi^\pm p$ scattering data. Kroll [2] determined the neutral pion coupling constant to $g^2_{\pi^0} = 14.52 \pm 0.40$, from analysis of pp scattering data by means of forward dispersion relations. In the early 1990's the Nijmegen group [3–5] found substantially smaller values for the coupling constants, on the basis of extensive and global energy-dependent partial-wave analyses (PWA) of nucleon-nucleon (NN) scattering data. They obtained the values $g^2_{\pi^0} = 13.47 \pm 0.11$ and $g^2_{\pi^\pm} = 13.58 \pm 0.05$. Similar coupling constants, with values around $g^2_\pi = 13.7$, have been found by the Virginia Tech group [6–8] from analysis of both $\pi^\pm N$ and NN data. Recently, Meissner and Henley [9] have estimated the charge dependence of the coupling constant due to π-η mixing and the u-d quark mass difference. They find that $g^2_{\pi^0}$ is expected to be a few % larger than $g^2_{\pi^\pm}$. These results have stimulated an intense debate, and it has forced a critical reappraisal of the entire reasoning on which the previous values were based. Reviewing this issue, it has become evident that the basis for the standard text book value is weaker than previously thought. It has therefore become urgent to deter-

*Present address: Gammadata AB, Box 15120, S-75015 Uppsala, Sweden.
†Present address: Tandem Accelerator Laboratory, Uppsala University, Box 535, S-75121 Uppsala, Sweden.
‡Present address: National Defense Research Establishment, Dept. 41, S-17290 Stockholm, Sweden.

mine $g^2_{\pi^\pm}$ and $g^2_{\pi^0}$ to high precision, convincingly and model independently [10].

In the analysis by the Nijmegen group [5] the determination of the coupling constant appears to be insensitive to the backward np cross section. In our work at 162 MeV [11], we have explicitly demonstrated the contrary using ''pseudo data'' generated from models in common use, including the Nijmegen potential [12]. The experimental normalization of the cross section is, however, crucial to the sensitivity and this has been a notorious problem in the past. Most groups working with energy-dependent PWA's have therefore chosen to let the normalization of individual data sets float more or less freely. Once this is done, the direct sensitivity to the np cross section might be lost, and as a consequence, the coupling constant can depend diffusely on many observables. With this procedure, the bulk of the large np data base has no direct experimental cross section scale outside the low-energy region, since polarization data rely on ratios. The potential dangers are obvious, even when extreme care is exercised.

Our conclusion from this discussion is that precision data of the differential np cross section in the backward hemisphere should be one of the best places in the NN sector to determine the charged coupling constant. In our recent work [11,13], we have shown that it is both the *shape* of the angular distribution at the most backward angles, and the *absolute normalization* of the data, that are of crucial importance in this context.

Moreover, the np scattering cross section, in particular at 180°, is of utmost importance for many applications of today, including medicine and accelerator-driven transmutation technologies. The reason is that this cross section is considered as a primary standard for measurements of other neutron-induced cross sections. Large uncertainties for such an important cross section are therefore unacceptable.

We have previously measured the relative differential np scattering cross section with high precision in the center-of-mass (c.m.) angular range $120°-180°$ at energies of 96 MeV [14] and 162 MeV [11] by detecting the recoil protons. We found significant deviations when comparing our data with other measurements, as well as with theoretical models for the NN interaction. This is especially true for the angular range $150°-180°$, where our data are much steeper than most previous data and model predictions. The discrepancy amounts to as much as 10–15% at 180°. A study of the np scattering data base up to the present date [15] shows that the data seem to fall into two main families with respect to the angular shape. The first one is dominated by the Bonner *et al.* data [16], which have a flattish angular distribution at backward angles. The second one, which includes our measurements and the Hürster *et al.* [17] data, have a steeper angular shape.

Since our measurements were relative, and only covered about one third of the total angular range, we extrapolated the data by using the Arndt energy-dependent phase shift solution VZ40 [7,18]. In that way we could normalize the absolute scale to the total np cross section, which has been measured very accurately [19,20]. We estimated that this procedure introduced a normalization uncertainty of about 4%, in addition to statistical and other uncertainties. The normalization uncertainty could in principle be brought down to the error of the experimental total cross section, i.e., about 1%, by measuring the full angular distribution. This involves, however, the difficult problem of detecting the scattered neutron in the forward hemisphere, since the recoil proton has too low energy to be reliably detected. But also a limited extension of the covered angular range would make the extrapolation safer, and thus bring down this uncertainty. Particularly, it is of great value to cover the region around 90°, where the solid angle element is at its maximum.

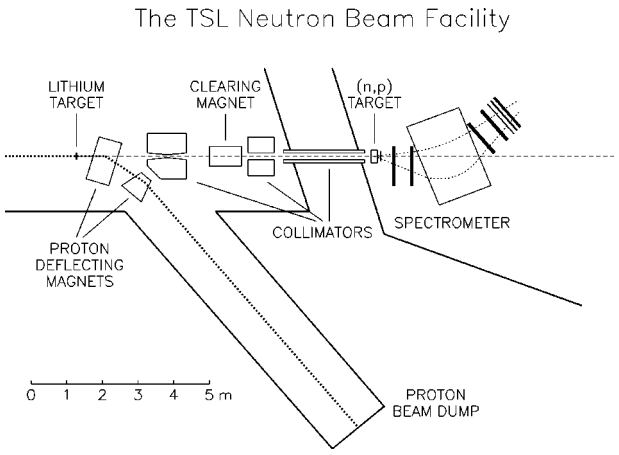

FIG. 1. Overview of the Uppsala neutron beam facility. The neutron production, shielding, and collimation are shown, as well as the magnetic spectrometer arrangement.

These arguments have motivated an extension of our previous data to cover a larger angular range, and to improve on the normalization. Thus, in this paper we present new measurements of the np differential scattering cross section at 162 MeV in the angular range $\theta_{\text{c.m.}}=72°-180°$, performed using the neutron beam facility at the The Svedberg Laboratory (TSL) in Uppsala. Special attention was paid to the precision of the data, and particularly to the absolute normalization.

A description of the experimental arrangement is given in Sec. II, while the procedure of the data reduction is treated in Sec. III. The experimental results are presented in Sec. IV, together with a detailed discussion of uncertainties and the normalization procedure. The determination of the πNN coupling constant from our np data is discussed in Sec. V, and finally, a summary and the conclusions are given in Sec. VI.

II. EXPERIMENTAL ARRANGEMENT

The experimental setup has been described in detail in a recent publication [21], and only a short summary will be given here, together with a more detailed description of the special arrangements used for this particular measurement.

An overview of the TSL neutron beam facility is shown in Fig. 1. Neutrons were produced by the $^7\text{Li}(p,n)^7\text{Be}$ reaction at 0°, which gives a quasimonoenergetic neutron beam, originating from the unresolved transitions to the ground state and first excited state ($E_x=0.43$ MeV) in ^{7}Be. In addition, there is an almost flat low-energy tail in the neutron spectrum. Lithium discs, enriched to 99.98% in ^{7}Li, and having thicknesses of 427 mg/cm^2 and 801 mg/cm^2 for the angular regions $\theta_{\text{c.m.}}=118°-180°$ and $\theta_{\text{c.m.}}=72°-130°$,

TABLE I. Experimental parameters for the different magnet settings.

Setting	Angular range (c.m.) (deg)	Li-target thickness (mg/cm^2)	Magnetic field (T)	Vertical acceptance (deg)	Energy resolution, FWHM (MeV)	Angular resolution (lab), rms (deg)
1	73−107	801	0.70	±0.8	5.3−7.0	0.6–1.1
2	89−129	801	0.80	±0.8	4.2−5.3	0.4–0.7
3	119−153	427	0.85	±0.8	3.1−4.5	0.4–0.5
4	137−167	427	1.20	±0.8	2.9−3.4	0.3–0.4
5	151−179	427	1.25	±1.0	3.0−3.2	0.3–0.4

respectively, were bombarded with a proton beam of a few hundred nA from the cyclotron. The neutron beam was defined by a system of three collimators, where the first one consisted of a 1.1 m long iron cylinder. The vacuum system was terminated after this collimator with a 1.0 mm thick aluminium plate. Charged particles produced in this plate and along the first collimator were deflected by a clearing dipole magnet. The second collimator was made of sandwiched iron and paraffin slabs, while the third one contained iron only. The total length of these two was about 3 m.

The diameter of the neutron beam at the np target position, located 8 m from the neutron production target, was 7 cm, which corresponds to a solid angle of 60 μsr. Typically, the neutron yield was of the order of 10^5 s^{-1} over the full target area in all runs. The energy of the centroid of the main peak in the neutron spectrum was determined to 162 ±1MeV. The finite width of this peak was caused by the energy spread of the proton beam, which was of the order of 0.3 MeV [full width at half maximum (FWHM)], and the straggling in the neutron production target, resulting in a total energy spread for the two target thicknesses of 1.3 and 2.3 MeV (FWHM), respectively. The unaffected neutron beam was dumped in a tunnel about 10 m after the spectrometer. There was essentially no background in the experimental hall, due to the very good shielding between the proton beam dump and the experimental area.

To maximize the count rate, the np target should contain as much material as possible, without impairing the energy resolution. Therefore, a sandwiched multitarget system was used, in which sheets of target material were interspaced by multiwire proportional chambers (MWPC's). In this way, it was possible to determine in which layer the reaction took place, and corrections for the energy loss in the subsequent targets could be applied in the off-line analysis. The multitarget box contained in total nine MWPC's, each having an efficiency of ⩾99%. The cathode planes were made of 6 μm polypropylene foils, coated with a 0.08 μm thick layer of aluminum. To optimize the background conditions, a hydrogen-free counting gas, consisting of a mixture of 80% argon and 20% CO_2, was used. When performing the present experiment, the nonhydrogen background originating from the empty target box was found to be less than 0.1%, and was therefore neglected. During the measurements, the first two MWPC planes provided a veto signal for rejection of the few charged particles that contaminated the neutron beam. The target box was filled with five 100 mg/cm^2 thick CH_2 and two 185 mg/cm^2 thick carbon targets. The carbon layers were included for subtraction of the $^{12}C(n,p)$ spectrum, which interferes with the np scattering in part of the angular region studied. The targets were stacked in the following (downstream) order: two CH_2, two carbon, and three CH_2 layers.

The momenta of the recoil protons were determined by a spectrometer, consisting of an H-shaped dipole magnet and four drift chambers (DCH's), two in front of and two behind the magnet. The scattering angles were determined by the trajectories through the first two DCH's. The spectrometer could be rotated around a pivot point, located just below the center of the target box, to cover different angular regions. The magnet had a pole face area of 90×120 cm^2 and a pole gap of 14 cm, subtending a solid angle of about 14 msr, as seen from the target. The field was determined by NMR to an accuracy of ±1G. With one position and one magnetic field setting, the spectrometer had a horizontal angular acceptance of about 15° in the laboratory system. To minimize the effects of multiple Coulomb scattering along the trajectories, helium bags were placed in the pole gap and between the two DCH's in front of the magnet.

The DCH's were of double sense-wire type with two-dimensional readout [22]. The detection area was 192×960 mm^2, divided into 40 horizontal and 8 vertical drift cells, each being 24 mm wide. The chamber windows were made of 25 μm thick mylar foils. The DCH counting gas was a mixture of 50% argon and 50% ethane, which has the advantage that the drift time is insensitive to small changes in the mixing ratio or in the voltage. The position resolution of each DCH was 0.3 mm (FWHM) for both the vertical and the horizontal coordinates. The detection efficiency for a single DCH plane was typically ⩾98%.

For the most backward angles, i.e., $\theta_{\text{c.m.}}=118°-180°$, a trigger signal for the data acquisition system was generated by a triple coincidence between two large plastic scintillators, being 4 and 10 mm thick, respectively, located behind the last DCH, and a thin 1 mm scintillator, positioned immediately after the multitarget box. In the angular region $\theta_{\text{c.m.}}=72°-130°$, a 2 mm thick scintillator was added as the first layer of the telescope behind the magnet. A double coincidence between the 1 and 2 mm thick scintillators was used as the trigger in this case, in order not to lose events by absorption in the thicker scintillators at these lower proton energies. The timing signal from the trigger, determined by the small 1 mm plastic scintillator, was used as the common stop for the drift time of the DCH's.

Measurements were performed over the proton angular range $\theta_{\text{lab}}=0°-54°$ by using five different settings of the spectrometer position, as is shown in Table I, where some relevant experimental parameters are given. These settings were chosen to give large angular overlaps. The multitarget

box was always rotated to be parallel with the first DCH, in order to minimize the target thickness seen by the recoil proton. Depending on the magnet position and the field setting, the lithium target thickness, and the angular region of interest, the energy resolution in the measured spectra was 2.9−7.0 MeV (FWHM). The angular resolution due to multiple Coulomb scattering, mainly in the target foils, was estimated to be 0.3°−1.1° (rms). The best energy and angular resolution was, however, obtained in the most important angular region, i.e., $\theta_{\text{c.m.}} = 140° - 180°$ (see Table I).

The data acquisition system consisted of a VME-bus configuration in conjunction with CAMAC and NIM electronic modules. For each event the time information from the DCH's and the MWPC's of the multitarget box, together with the linear signals from the scintillators, were stored on magnetic tape. Preliminary spectra could also be monitored on line.

III. DATA REDUCTION AND CORRECTIONS

The data were analyzed off line on an event-by-event basis. Before an event was accepted, a number of tests were applied. First, events originating from charged particles contaminating the neutron beam, and detected in the first two planes of the multitarget system, or produced in the thin scintillator just behind the target system, were removed. This could be done reliably because of the high efficiency of the MWPC's.

The energies of the charged particles from the targets were determined by an iterative ray-tracing procedure, using measured magnetic field maps and the position information from the DCH's. To this end, both the horizontal and vertical coordinate information of the first two DCH's were needed, together with the horizontal coordinate from one of the chambers after the magnet. If any of this information was lacking, the event was rejected. By using either the third or the fourth DCH, two energy values were obtained. By taking the difference between those values, a consistency check of the energy could be applied, and events with dubious energy determination could be rejected. This is illustrated in Fig. 2(a). If the ray-tracing iteration did not converge, or the particle trajectory was outside the magnetic field limits, the event was considered spurious and removed. Such events are mainly due to deuterons.

The scattering angle was determined by calculating the particle trajectory through the first two DCH's, using both the horizontal and vertical coordinate information. In this way we also account for scattering out of plane. To avoid complicated, angle-dependent, vertical acceptance corrections, software gates of $\pm 0.8°$ were applied on the vertical scattering angle, ensuring that all accepted particles could freely pass the magnet gap. For the highest magnetic field, the vertical focusing by the fringe field allowed a slightly larger acceptance of $\pm 1.0°$ to be used. It should be noted that because of the extended target and beam spot size, at least three drift cells of the DCH's contribute at each angle, thus smearing any effects of inefficiencies that in principle could be present within a drift cell. The reaction coordinates at the target planes were also determined from the particle trajectories through the first DCH's. Thus, it could be checked that the charged particle for each event originated from the area of the neutron beam spot, and the small number of spurious events outside this area could be rejected, as is shown in Fig. 2(b).

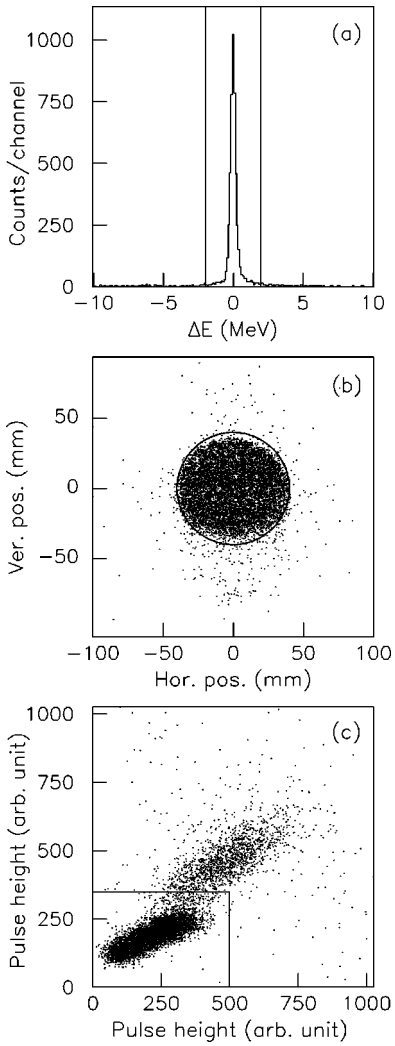

FIG. 2. (a) Difference of proton energies determined using DCH 3 or 4. The vertical lines show the gate for accepted events. (b) Scatter plot of the reaction vertices at target plane 5. A circular gate was applied to reject events that do not originate from the target. (c) Scatter plot of pulse heights from the 4 mm versus the 10 mm thick large plastic scintillators. The solid line represents the gate used to reject most of the deuterons.

Together with information on the particle momentum, the pulse heights from two of the large scintillators were used for particle identification, enabling separation of protons from other charged particles, mostly deuterons. This is illustrated in Fig. 2(c), where the pulse heights of the 4 mm and 10 mm thick scintillators are plotted versus each other, for events with a momentum corresponding to a proton energy in the range 140−180 MeV. The protons are seen in the bottom left corner, while the deuterons give slightly larger pulse heights. Also shown is the cut used to reject most of the deuterons (solid line). Finally, all accepted events were stored in matrices with angular and energy binning in the laboratory system of 1° and 0.25 MeV, respectively.

Before extracting the hydrogen peak content, the carbon contribution to the CH_2 spectra was subtracted. This is illustrated for a few selected angles in Fig. 3, where an energy

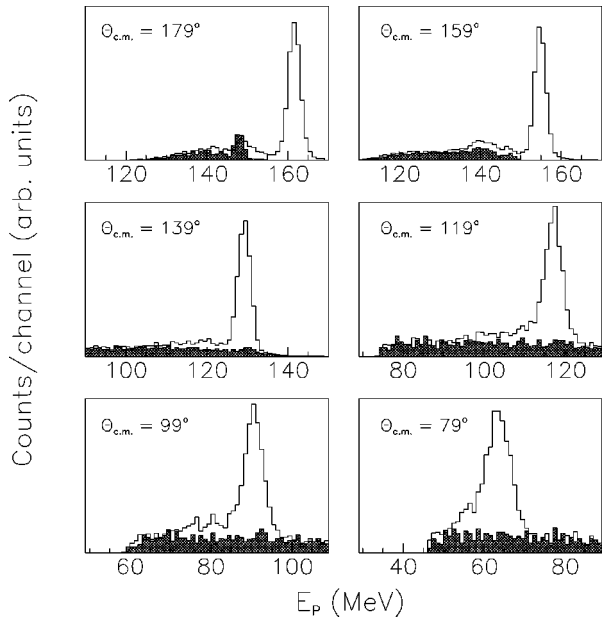

FIG. 3. Proton energy spectra from CH_2 (open histograms) and carbon (cross-hatched histograms) targets, respectively, at various scattering angles. The part of the CH_2 spectra at lower energies not accounted for by the carbon contribution originates from *np* scattering of neutrons from the low-energy neutron tail.

binning of 1 MeV was used. The open histograms represent the energy spectra from the CH_2 foils, while the cross hatched histograms are those of the pure carbon targets, after normalization to the same number of target nuclei. The high efficiency of the MWPC's ensured a very precise identification of the various target layers (CH_2 or C). This could also be verified by comparing the spectra from the CH_2 layers positioned before and after the carbon targets. As can be seen in the figure, there is no interference from the carbon background at extreme backward angles due to the strongly negative Q value of the $^{12}C(n,p)^{12}B$ reaction (-12.6 MeV), whereas it contributes below about $\theta_{\text{c.m.}}=145°$ because of the difference in kinematics. The carbon spectra account for most of the background, and the small remainder on the left side of the peak is attributed to scattering of neutrons from the low-energy tail of the incident neutron beam. There is an indication of a small peak in the CH_2 spectra at 10-15 MeV below the main peak, which is in the same region as the peak structure in the tail of the $^7Li(p,n)$ spectrum (cf. Fig. 4).

The *np* scattering peak contents were determined by integration. To take into account the variation of the energy resolution with scattering angle, different energy windows had to be used. To reduce the systematic errors introduced by this procedure, the peak widths had to be defined in a consistent way. To this end, a Gaussian distribution was fitted to the *np* peak at each angle to determine the centroid and the width. The peak content was finally determined by integrating the data in a region of $\pm\Delta E$ around the centroid, where ΔE is the peak FWHM. With this definition, the carbon background amounted to maximum 25% of the hydrogen peak, which occurred for the largest recoil angles.

Since the width of the *np* peak varies with angle, the low-energy continuum, originating from the $^7Li(p,n)$ reaction, will give different contributions at different angles. To correct the data for this effect, we used experimental neutron spectra for the $^7Li(p,n)$ reaction determined by Byrd and Sailor [23]. These authors give 0° data at $E_p=90.1$ and 139.9 MeV, which have a resolution of 1.11 and 1.72 MeV (FWHM), respectively, i.e., much better than in the present experiment. In these spectra, a minimum is clearly seen between the rather flat continuum and the full-energy peak (see Fig. 4). To estimate the continuum contribution under the peak, a straight line was drawn from the minimum to the last point on the high-energy side of the peak (dotted line). The dashed line corresponds to the peak after subtraction of the continuum, and the solid line is the sum of the two contributions. To simulate the finite resolution of our experiment, both parts of the Byrd and Sailor spectra were folded with Gaussian resolution functions, having widths from 1 to 10 MeV (FWHM). From these folded spectra, the continuum contribution to the peak, as defined above, could be determined as a function of the peak width. The resulting correction factors at the two energies are shown as circles in Fig. 5. The solid line is a fit to the two data sets, and it is assumed that this correction is valid in the range 90-160 MeV. It can be seen from the figure that the maximum correction to our data, i.e., for $\Gamma=\Delta E=7$MeV (FWHM), is about 5%.

As the measurements are relative, recoil proton absorption effects should not be important to leading order. But since the energy of the recoil protons varies with scattering angle, the variation of the absorption with energy has to be taken into account. The removal of protons can be caused by elastic scattering or by nonelastic reactions. To first order, the in and out scattering of particles are expected to cancel, and thus only nonelastic losses have to be considered. To that end, we calculated these losses in targets, detectors, and helium gas, using the total reaction cross sections given by Carlson [24]. It turned out that the proton attenuation is only important in the angular region $\theta_{\text{c.m.}}=72°-100°$, and the maximum correction amounts to 1.6% (for the 73° data point).

IV. EXPERIMENTAL RESULTS

A. Relative cross sections

The problem is now to link the relative differential cross sections for the five different magnetic settings. Usually this is achieved using an external neutron beam monitor, which in principle could introduce extra systematic errors caused by monitor drifts, etc. Such problems can be avoided using the overlapping regions as an internal monitor, if these regions contain sufficiently good statistics. We have matched the five data sets pairwise in each of the overlapping regions using a minimum χ^2 criterion

$$\chi_j^2=\sum_{i=1}^{N_j}\frac{(x_i-k_jy_i)^2}{(\Delta x_i)^2+k_j^2(\Delta y_i)^2}, \tag{1}$$

where x_i and y_i are the relative cross sections of data sets x and y at angle i, Δx_i and Δy_i are the corresponding uncertainties, k_j is the matching coefficient of data set y, and N_j is the number of points in the overlapping region j. The N_j and χ_j^2 per degree of freedom for the four overlapping regions are given in Table II. The coefficients k_j are almost

TABLE II. Overlapping angular regions, number of angle bins in these regions, χ^2 per degree of freedom, and the relative uncertainty of the matching coefficients.

Overlap region (deg c.m.)	j	N_j	$\chi_j^2/(N_j-1)$	$\Delta k_j/k_j$ (%)
89−107	1	10	3.4	±1.6
119−129	2	6	0.69	±1.6
137−153	3	9	0.23	±1.1
151−167	4	9	2.4	±0.8

uncorrelated, since there is no overlap between three or more data sets, except between $\theta_{\text{c.m.}}=151°$ and 153°, where three data sets overlap. The result of this matching is shown in the c.m. system in Fig. 6. The agreement in the overlapping regions is generally very good, although the individual points scatter at the few percent level. Final relative np scattering cross sections were obtained by averaging the data from the different data sets in each 2° angular bin.

Many sources of uncertainties contribute to the total errors in the relative cross section. These errors are of both random and systematic character. Since the measurement is relative, only those systematic errors that affect the shape of the angular distribution have to be considered. A complication, however, is that some of the systematic errors affect only a narrow angular interval, while others are important for a large fraction of the angular distribution. Thus, the different systematic errors cannot easily be fully disentangled.

The random error is dominated by counting statistics, and amounts to between 1.0 and 3.8%, including the contribution from the carbon background subtraction. The smaller value is valid for scattering angles close to 180°, which is the most important region for, e.g., the determination of the πNN coupling constant. Another small, random error is introduced when defining the boundaries in the peak integration procedure, originating from bin truncation. The error contribution from this procedure is at most 0.6% per point.

There are several contributions to the total systematic error. In the off-line analysis, up to 0.6% proton events are cut

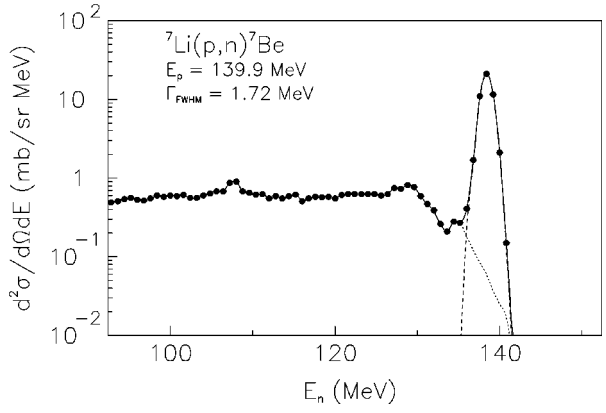

FIG. 4. Experimental 0° neutron spectrum for the ^{7}Li(p,n) reaction at $E_p=139.9$ MeV [23] (filled circles). The estimated continuum contribution to the full-energy peak is shown as a dotted line. The dashed line corresponds to the full-energy peak after subtraction of the continuum, while the solid line is the sum of the two contributions.

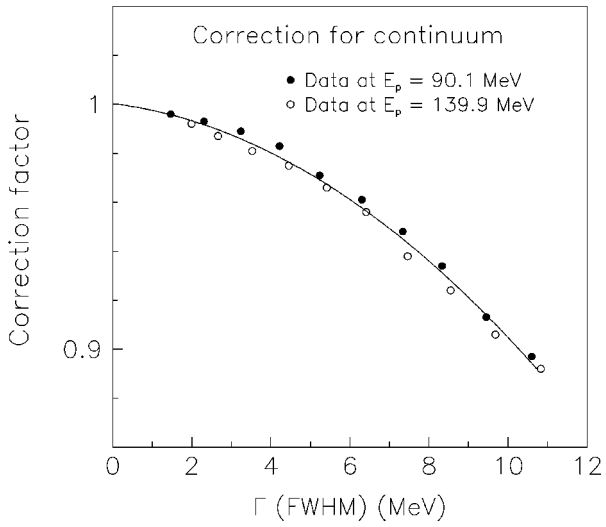

FIG. 5. Low-energy continuum correction of the full-energy np peak versus energy resolution. Shown are data at $E_p=90.1$ MeV (filled circles) and 139.9 MeV (open circles) [23]. The solid line is a fit to the two data sets.

in the particle identification analysis [see Fig. 2(c)]. However, most of those protons are of low energy and come from the ^{12}C(n,p) reaction, and therefore do not affect the total np angular distribution. The remaining part can at most give an error of about 0.1% per point.

The most important contribution to the systematic error is related to the subtraction of the background from carbon in the CH_2 samples. First, the uncertainty in the relative target thicknesses, which is estimated to be less than 4%, introduces an error in the extracted cross sections. This error is about 1% at $\theta_{\text{c.m.}}=73°$ and decreases with increasing angle until it vanishes at about 150°. Second, the relative energy uncertainty between the CH_2 and carbon spectra, which originates from the energy loss correction applied for each

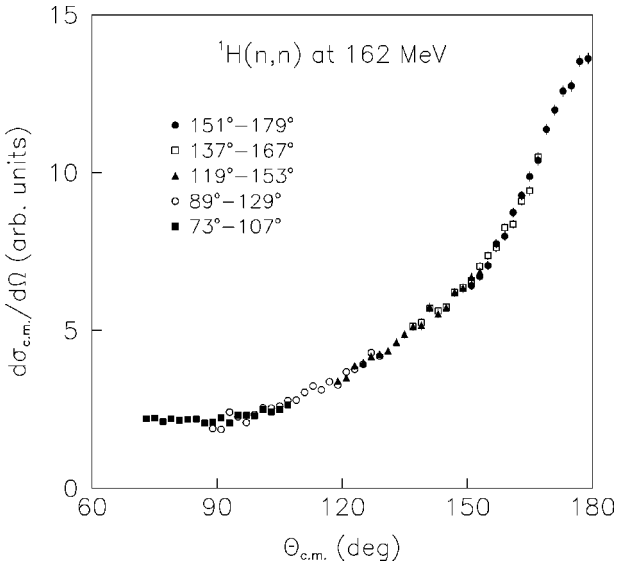

FIG. 6. Relative differential cross sections at $E_n=162$ MeV. The different symbols represent data from the five magnetic settings. These were normalized to each other in the overlapping regions.

target type and plane, causes an error in the angular range $135°-155°$, where the carbon background partly interferes with the hydrogen peak. An estimated uncertainty of ± 1MeV in the relative energy of protons from CH_2 and carbon yields an error in the background subtraction, which in turn causes an error in the *np* cross section of at most 1.8%. Above 155°, the hydrogen peak is well separated from the carbon spectrum, and below 135° the hydrogen peak is superimposed on a rather flat carbon continuum, and hence a relative energy uncertainty will not affect the data in these regions.

The correction ($<5\%$) for the contribution from the low-energy continuum of the ^{7}Li(p,n) spectrum to the *np* scattering peak introduces a systematic uncertainty that varies with the peak width, or, with angle. Assuming a relative uncertainty of 10% in the correction, an error in the data of at most 0.5% arises. The error from the small correction due to the energy-dependent attenuation of the protons is estimated to be less than 0.5%.

When summing all the mentioned effects, the total systematic error varies from 0.3 to 1.9 % in the measured angular region. The maximum error is found in the range $\theta_{\text{c.m.}}=135°-155°$.

In addition to the random and systematic errors discussed, the shape of the full angular distribution is affected by the matching of the five data sets. The uncertainties of the fitted coefficients k_j, emerging mainly from the finite counting statistics, are given in Table II. A quadratic addition results in a shape error of $\pm 2.6\%$ between the first and fifth data sets, i.e., in the 73° to 179° cross section ratio.

B. Normalization procedure

Absolute *np* scattering cross sections were obtained using the total *np* cross section, which is assumed to be experimentally well known. If our measurement had covered the full angular range, a normalization of the angle-integrated cross section to σ_T would have been straightforward, since other reaction channels are negligible at 162 MeV. With the lack of data at forward angles, we instead consider our experiment as a measurement of a *fraction* of the total cross section, i.e., the part between 72° and 180°. By using a number of PWA's or potential models found in the literature, which are based on the bulk of the world *np* data, we can get an estimate of the magnitude F of this fraction, and thus correct the total cross section to which our data should be normalized. Thus, we require that the integral over solid angle of our data should be equal to

$$\sigma_{72°-180°}=\int_{72°}^{180°}\frac{d\sigma}{d\Omega}d\Omega=F\sigma_T^{\text{exp}}, \tag{2}$$

where

$$F=\sigma_{72°-180°}^{\text{PWA}}/\sigma_T^{\text{PWA}}. \tag{3}$$

The total cross section has recently been measured to high accuracy at Los Alamos by Lisowski *et al.* [19] and at PSI by Grundies *et al.* [20]. The statistical errors of these data are very small, while the systematic uncertainty in the former measurement is less than 1% and in the latter below 1.5%. To interpolate between these precision points, the Nijmegen energy-dependent PWA NI93 (Ref. [25]) was fitted to the data in the 100–250 MeV region, as is illustrated in Fig. 7. A slight renormalization of 0.995 was needed to obtain a good fit. Also other PWA's and potentials were tested, but it was found that the NI93 PWA best represented the energy dependence of the data. The resulting total cross section at 162 MeV is

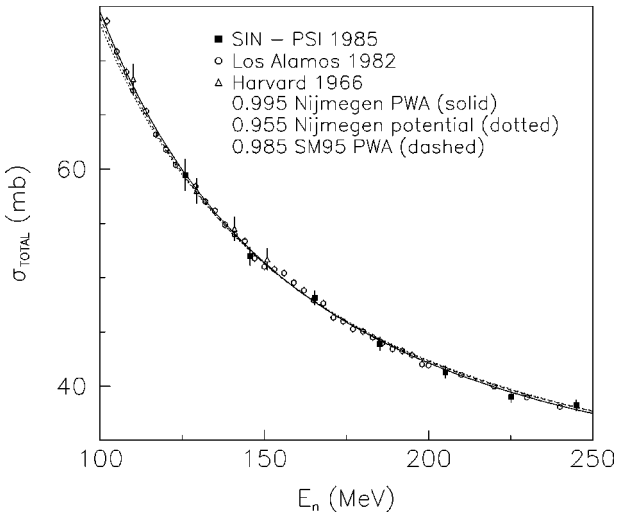

FIG. 7. Total *np* cross section versus energy in the range 100–250 MeV. The different symbols represent experimental data [19,20,27], while the lines are from PWA's and *NN* potentials, renormalized to the data in the shown energy region.

$$\sigma_T^{\text{exp}}=48.47\pm 0.48\pm 0.22=48.47\pm 0.53\ \text{mb}, \tag{4}$$

where the first error corresponds to the 1% systematic error of the Lisowski data, and the second error is due to the 1 MeV neutron beam energy uncertainty, for which the total cross section has a slope of 0.46%/MeV.

To determine the fraction F of the total cross section covered in the experiment, we used information on the $72°-180°$ integrated differential cross section and total cross section from the PWA's SM95, VZ40, and VL40 of Arndt [7,18,26], and NI93 from Nijmegen [25]. VZ40, VL40, and NI93 are energy-dependent PWA's fitted to data in the 0–350 or 400 MeV region, while SM95 was obtained by fitting up to 1.6 GeV. The result is shown in Table III, where also integrated cross sections and fractions for the Paris [28], Bonn [29], and Nijmegen [12] potentials are given. As we believe that the PWA's are more reliable, since they describe the total cross section much better, the potential models were not included in the determination of F. For the final value of F we took the average value for the four PWA's mentioned, i.e., $F=0.636$. Thus, our data have been normalized to

$$\sigma_{72°-180°}^{\text{exp}}=F\sigma_T^{\text{exp}}=0.636\times 48.47=30.83\ \text{mb}. \tag{5}$$

The result is shown in Fig. 8(a), where the differential cross section, multiplied with the solid angle element $2\pi\sin\theta$, is shown. In this representation, each angle bin directly shows its contribution to the total cross section. It is obvious that at angles close to 180°, where the differential cross section is at maximum, the contribution to the total cross section is very small. Instead, it is the data in the region

TABLE III. Total cross sections (σ_T) and fraction values (F) of different PWA's and NN potentials.

PWA or potential	σ_T	$\sigma_{0°-72°}$	$\sigma_{72°-180°}$	$F=\sigma_{72°-180°}/\sigma_T$	$\sigma_T^{\rm exp}/\sigma_T$
SM95	49.06	18.52	30.54	0.6225	0.9880
VZ40	48.23	17.62	30.61	0.6347	1.0050
VL40	48.18	17.50	30.68	0.6368	1.0060
NI93	48.68	17.04	31.64	0.6500	0.9957
Average	48.54	17.67	30.87	0.6360	0.9987
Paris	51.22	18.04	33.18	0.6478	0.9463
Bonn	48.32	16.60	31.72	0.6565	1.0031
Nijmegen	50.74	18.15	32.59	0.6423	0.9553

$100°-160°$ that have a dominating impact on the normalization. Also shown in the figure are the angular distributions of the PWA's used to determine F, all slightly renormalized to the experimental total cross section of 48.47 mb. It is interesting to note that with this double-hump structure, any enhanced cross section in the region around 140° has to be compensated by a corresponding reduction around 40°, or vice versa, in order to conserve the total cross section. It is also obvious that the main difference between the various PWA's or potential models is found in the balance between the 40° and 140° humps. Thus, a future extension of precise data down to 30° would be of great value to disentangle this problem and ultimately settle the normalization.

The spread in F for the various PWA's or potential models could give an estimate of the precision of the normalization procedure. One can see from Table III that the maximum deviations occur for SM95 (-2.1%) and the Bonn potential ($+3.2\%$). From this comparison, we believe it is fair to estimate the normalization uncertainty to $\pm 2\%$. To this should be added the ''intrinsic'' uncertainty in $\sigma_T^{\rm exp}$ of 1.1%. Thus, we assign a total uncertainty of $\pm 2.3\%$ to the normalization of our data.

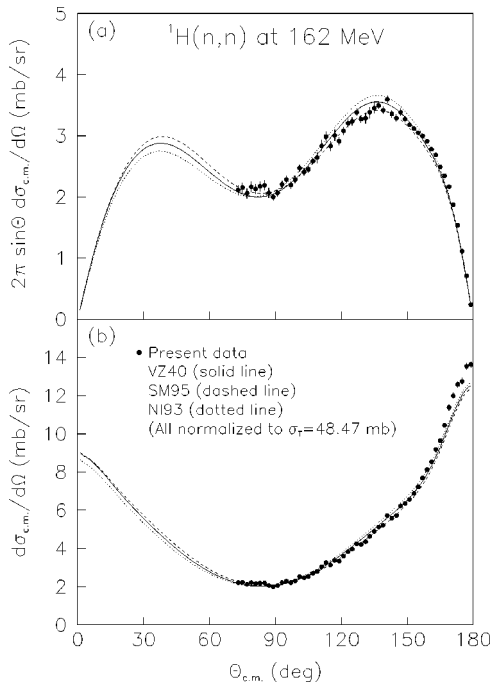

FIG. 8. Angular distributions for the SM95, VZ40 [7,18,26], and NI93 [12] PWA's, and the present experimental data (filled circles) at 162 MeV. The VL40 PWA solution of Arndt *et al.* is almost identical to VZ40 and is not shown for clarity. (a) Differential cross sections multiplied by the solid angle element $2\pi \sin\theta$. (b) Differential cross sections for np scattering.

C. Absolute cross sections

The resulting experimental differential cross sections from the present work are given in Table IV, and are also shown as filled circles in Fig. 8(b). The errors given are the quadratic sums of the statistical and systematic uncertainty contributions to the relative cross sections, as discussed above. To this should be added errors from two sources: (1) the shape uncertainty of $\pm 2.6\%$ in the 73° to 179° cross section ratio, originating from the internal matching of the five data sets and (2) the overall normalization error of $\pm 2.3\%$. These two errors are, however, correlated. With the normalization method used, a different shape of the angular distribution gives a different normalization. Within the given shape uncertainty, one can get an angular distribution that is, e.g., flatter by 2.6%. After normalization, this leads to changes of $+1.3\%$ in the first (most forward) data set and of -1.3% in the fifth (most backward) data set, and less for the intermediate sets. With a steeper angular distribution the signs of the changes are reversed. Also shown in the figure are the PWA's used for the normalization. It is immediately seen that the present data set is steeper than the PWA's in the $150°-180°$ angular region, while they are well described from 70° to 150°, especially by SM95.

The present data have a normalization that on the average is about 3% lower compared to the preliminary data in the $120°-180°$ range [11]. This renormalization is well within the normalization error of 4% stated in that work.

The result of the present experiment is compared with previous measurements at energies close to 162 MeV in Fig. 9(a). The Measday [30] and Palmieri and Wolfe [31] data were originally normalized to the Yale PWA YLAN4MP [32], but have been renormalized to VZ40 [7,18] by us, using factors of 0.96 and 0.88, respectively. The Bonner *et al.* data [16] at 162 MeV are only relative, and have been made absolute by normalization to VZ40. The forward-angle data by Bersbach, Mischke, and Devlin [33] are given as absolute cross sections by measuring the neutron yield in the beam. As can be seen, the present data are much steeper in the

TABLE IV. Differential cross sections of the present work for np scattering at 162 MeV. The given uncertainties are a combination of statistical and systematic errors. The errors from the internal matching of the five data sets and the overall normalization are not included.

$\theta_{\text{c.m.}}$ (deg)	$d\sigma/d\Omega$ (mb/sr)	$\theta_{\text{c.m.}}$ (deg)	$d\sigma/d\Omega$ (mb/sr)	$\theta_{\text{c.m.}}$ (deg)	$d\sigma/d\Omega$ (mb/sr)
73.0	2.207±0.089	109.0	2.795±0.094	145.0	5.737±0.111
75.0	2.226±0.087	111.0	3.041±0.098	147.0	6.214±0.106
77.0	2.110±0.084	113.0	3.245±0.098	149.0	6.352±0.099
79.0	2.206±0.083	115.0	3.125±0.098	151.0	6.559±0.076
81.0	2.157±0.080	117.0	3.375±0.102	153.0	6.870±0.074
83.0	2.189±0.081	119.0	3.333±0.074	155.0	7.216±0.089
85.0	2.199±0.080	121.0	3.596±0.076	157.0	7.680±0.091
87.0	2.069±0.079	123.0	3.823±0.077	159.0	8.128±0.093
89.0	1.999±0.056	125.0	3.953±0.078	161.0	8.539±0.096
91.0	2.065±0.057	127.0	4.238±0.080	163.0	9.183±0.099
93.0	2.207±0.058	129.0	4.211±0.079	165.0	9.635±0.101
95.0	2.297±0.058	131.0	4.355±0.119	167.0	10.446±0.105
97.0	2.211±0.058	133.0	4.624±0.122	169.0	11.370±0.160
99.0	2.314±0.059	135.0	4.883±0.126	171.0	11.987±0.163
101.0	2.518±0.060	137.0	5.129±0.087	173.0	12.582±0.167
103.0	2.475±0.059	139.0	5.215±0.090	175.0	12.743±0.166
105.0	2.539±0.059	141.0	5.716±0.099	177.0	13.531±0.163
107.0	2.704±0.061	143.0	5.577±0.102	179.0	13.615±0.164

$150°-180°$ region, and the discrepancies amount to as much as 10–15% at 180°.

In Fig. 9(b) the data are compared with three NN potential models, namely the Paris [28], Bonn [29], and Nijmegen [12] potentials. The Paris and Nijmegen potentials are similar and describe the data well close to 180°, while a 10% overprediction is seen in the $100°-160°$ region. On the other hand, the ratio of the 180° cross section to that in the $70°-90°$ region is well described by the models. One should keep in mind, however, that both of these potentials overpredict the total cross section by 5% (see Table III). The Bonn potential, which gives a good value for the total cross section, coincides with the other models and the data around $70°-90°$, while it shows an underprediction of 10% at 180°. It can also be seen that the data set is steeper than all three models in the $150°-180°$ region.

To be able to compare the present results with data at other energies, the differential cross sections $d\sigma/d\Omega$ have been converted into $d\sigma/dt$, where t is the Mandelstam variable, corresponding to the square of the c.m. charge exchange momentum transfer. If p_n denotes the neutron incident laboratory momentum, the product

$$p_n^2 \frac{d\sigma}{dt} \tag{6}$$

when plotted versus t, should look the same for all data sets only if the pion pole term plays a significant role. Deviations from such a universal behavior could be attributed to, e.g., effects of other interactions, such as multiple pion exchange. Since a majority of the data sets have either a floating normalization, or a large uncertainty in the absolute scale, we renormalized the different data sets to agree at $t=0$, which corresponds to np scattering at 180°. This was done by fitting the data according to an empirical two-exponential form [34]

$$\frac{d\sigma}{dt} = \alpha_1 e^{\beta_1 t} + \alpha_2 e^{\beta_2 t}, \tag{7}$$

which has been frequently used previously when comparing different data sets.

A few data sets are plotted in this way together with our data in Fig. 10. The plots cover the range up to $t=0.06$ $(\text{GeV}/c)^2$, corresponding to np scattering angles of about 127° at 160 MeV and 153° at 580 MeV. The fit to the present data is shown as a solid line, whereas the fits to other data are represented by dashed lines. All the fits were performed up to $t=0.08$ $(\text{GeV}/c)^2$. The left panel shows data of Bonner *et al.* [16] from 212 to 588 MeV. At the lower energies, these data are less steep than the present data set, just as was the case at 162 MeV [Fig. 9(a)]. The deviation is of the order of 15%. The agreement improves, however, when going to higher energies. The 451 MeV data set agrees well with the present one up to $t=0.03(\text{GeV}/c)^2$, and at 588 MeV the Bonner data set is even steeper than ours at small t. The right panel shows data of Hürster *et al.* [17] at approximately the same energies. These data show a remarkable agreement with the present ones at all energies, with shape deviations within a few percent. The Hürster data, which originally covered the angular range $144°-180°$, have re-

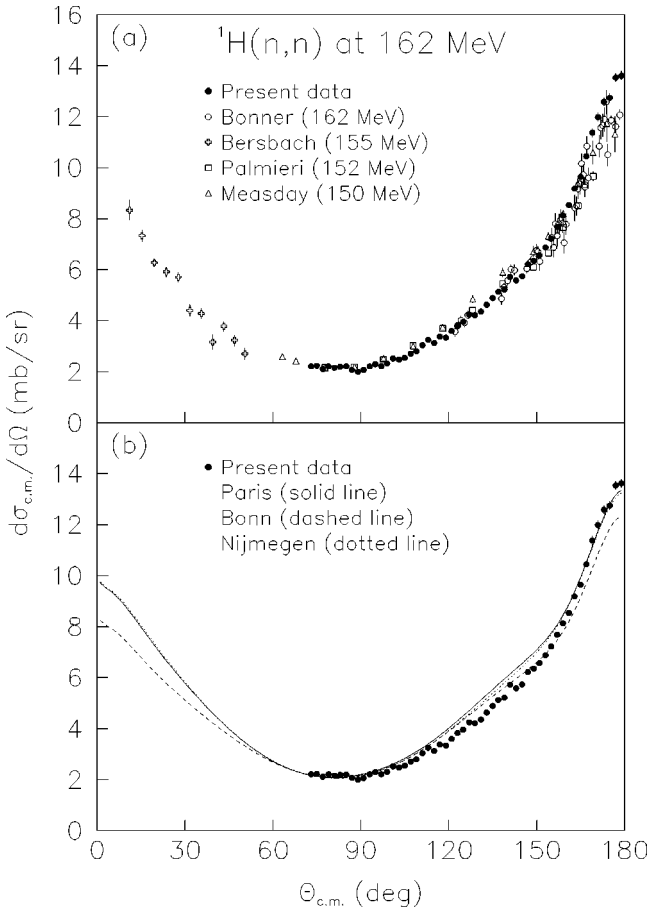

FIG. 9. (a) Differential np scattering cross sections of the present work (filled circles). Also plotted are other data from the literature at energies close to 162 MeV [16,30,31,33]. (b) The present differential cross sections plotted together with the Paris [28], Bonn [29], and Nijmegen [12] NN potentials.

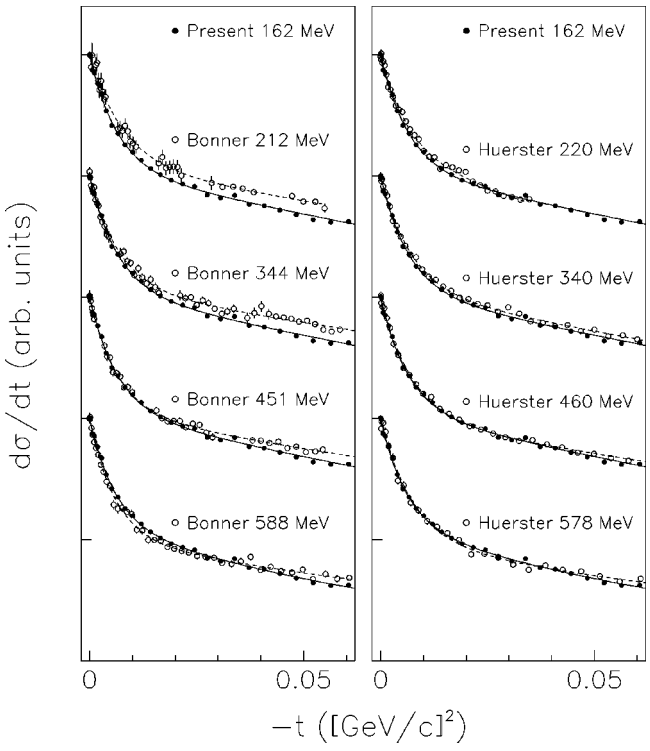

FIG. 10. Differential np scattering cross sections for data at various energies [16,17] plotted as $d\sigma/dt$ versus t. The different data sets were normalized to each other at $t=0$.

cently been extended down to 80° [35], and it will be extremely interesting to perform a new comparison when these data have been published.

V. THE πNN COUPLING CONSTANT DETERMINATION

The most stringent present requirement for precision in the pion-nucleon coupling constant is set by the Goldberger-Treiman (GT) relation [36]

$$g(q^2=0)=\frac{g_A M}{\sqrt{4\pi}f_\pi}, \tag{8}$$

where all quantities should be taken in the chiral limit of a vanishing pion mass. Here $g(q^2=0)$ is the πNN vertex function, taken at $q^2=0$. With the latest value for the axial coupling constant $g_A=1.266\pm0.004$ [37] and with the pion decay constant $f_\pi=92.42\pm0.26$ MeV [38] and M the average nucleon mass, this relation gives $g^2(q^2=0)=13.16\pm0.16$ using the physical values for all the other quantities. The error comes from the experimental uncertainty in g_A and f_π. The latest determination of g_A has increased it from the previous lower value $g^2(q^2=0)=12.81\pm0.12$ [13]. A precise test of the GT relation therefore requires that $g^2(q^2=0)$ be determined to somewhat better than 1%, assuming that the chiral corrections can be controlled to this level. The coupling constant is defined at the pion pole for $q^2=-m_\pi^2$ and not for $q^2=0$. It is then instructive to express the GT relation in terms of the coupling constant directly. A monopole form factor for the vertex with a cutoff Λ gives a g^2 increased by a factor $1+2m_\pi^2/\Lambda^2$, i.e., by 6% for $\Lambda=800$ MeV. This corresponds[1] to a $g^2_{\pi^\pm}\equiv g^2(q^2=-m_\pi^2)$ of about 14.0. One should note, however, that the GT discrepancy depends in addition on a low-energy chiral parameter, which cannot be determined from other reactions [39]. Presently, the GT relation is consistent with all values of the pion coupling under discussion.

It is in this perspective that we analyze the present data with the aim of extracting the πNN coupling with precision. The analysis is based on the fact that the charged pion exchange contributes importantly to the np charge exchange at small momentum transfers. This was realized already in 1958 by Chew, who suggested a model-independent extrapolation to the pion pole for the determination of the coupling constant (the Chew extrapolation procedure) [40,41]. It is based on a polynomial expansion in the square of the momentum transfer q^2. The basic idea is sound. However, it has

[1]Two different definitions of the coupling strength are frequently used, with different notation. The pseudovector coupling $f^2_{\pi^\pm}\sim0.08$ and the pseudoscalar $g^2_{\pi^\pm}\sim14$, are related by $g^2_{\pi^\pm}\equiv f^2_{\pi^\pm}(2M_p/m_{\pi^\pm})^2$, where M_p and $m_{\pi^\pm}$ are the proton and charged pion masses, respectively. Throughout this article the $g^2_{\pi^\pm}$ and $f^2_{\pi^\pm}$ include the $1/4\pi$ factor.

proved difficult to apply this method with precision. On the one hand, data have not been sufficiently accurate and, on the other, the method requires information on relatively high momentum transfers. The value of the polynomial expansion is then questionable. Improvements have therefore been introduced. In particular, Ashmore *et al.* have made explicit use of the pion Born terms with an additional phenomenological background term [42]. This simulates in part the important ρ exchange, which improves the convergence at the cost of some model dependence. Another approach is the difference method introduced previously in the first report on the present work [11] and also applied to $\bar{p}p$ charge exchange [43]. We take the attitude that it is an advantage in a precision and model-independent procedure to determine the value of the *difference* of the coupling with respect to its known value in an approximate model, rather than the full value directly. In this way we obtain a simpler procedure with suppression of contributions from higher momenta and one which is more readily amenable to tests of the systematic uncertainties in the method. This will be discussed in detail in the following.

Before proceeding with the discussion we make two important remarks. First, as already noticed in the previous section for energies up to 600 MeV, it is striking that the *np* unpolarized charge exchange cross sections in a very large range of energies from about 100 MeV to several GeV, have with only minor variation, similar shape and similar normalization (in the laboratory system). Consequently, these data contain essentially the same physical information as far as the extrapolation to the pion pole is concerned. Accurate information on the cross section at any one of these energies is therefore equivalent to such data at another energy. Only if systematic experimental effects can be ignored, is it advantageous to pool data from many energies so as to improve statistics. Second, it is essential to understand in some detail the nature of contributions to the cross section, their characteristic behavior and physical origin. This is so, even when a model-independent procedure is used in the analysis. This has not been done in the past, but it immediately clarifies which aspects must be handled with special care. We find in particular that the absolute normalization is crucial for the accurate determination of the coupling constant.

A. Pion exchange amplitudes

The total amplitudes and cross sections are defined in the usual fashion in terms of the five amplitudes a, b, c, d, e allowed by the invariance properties [44]. Both the c.m. unpolarized cross section and the polarization transfer one are incoherent combinations of five amplitudes

$$\frac{d\sigma}{d\Omega}(q^2)=\frac{1}{2}(|a|^2+|b|^2+|c|^2+|d|^2+|e|^2), \tag{9}$$

$$\frac{d\sigma}{d\Omega}(q^2)(1-K_{0nn0})=|b|^2+|d|^2, \tag{10}$$

where q^2 is the squared momentum transfer from the neutron to the proton.

Corresponding to these five amplitudes there are five regularized pion Born amplitudes with the coupling constant $g^2_{\pi^\pm}$ and with the r-space δ function subtracted [45], viz.,

$$a_\pi=\frac{g^2_{\pi^\pm}}{6\sqrt{s}}[F_0(p^2)+2F_c(q^2)],$$

$$b_\pi=\frac{g^2_{\pi^\pm}}{6\sqrt{s}}[-F_0(p^2)-6\Pi_c(q^2)F_c(q^2)+4F_c(q^2)],$$

$$c_\pi=\frac{g^2_{\pi^\pm}}{6\sqrt{s}}[-3\Pi_0(p^2)F_0(p^2)+2F_0(p^2)-2F_c(q^2)],$$

$$d_\pi=\frac{g^2_{\pi^\pm}}{2\sqrt{s}}[-\Pi_0(p^2)F_0(p^2)+2\Pi_c(q^2)F_c(q^2)],$$

$$e_\pi=0, \tag{11}$$

where we use the subscript 0 for π^0 and c for $\pi^\pm$ exchanges. The pion form factors $F(z^2)$ and the pion propagator $\Pi(z^2)$ are given by

$$F(z^2)\equiv\left(\frac{\Lambda^2-m_\pi^2}{z^2+\Lambda^2}\right)^2; \quad \Pi(z^2)\equiv\frac{z^2}{z^2+m_\pi^2}. \tag{12}$$

Here the momentum transfer corresponding to charged pion exchange is $q^2=2k^2(1+\cos\theta_{\text{c.m.}})$ with the c.m. momentum squared $k^2=MT_{\text{lab}}/2$. The momentum transfer corresponding to π^0 exchange is $p^2=2k^2(1-\cos\theta_{\text{c.m.}})$. The charged pion mass is denoted by m_π and the range of the form factor is chosen to be $\Lambda=800$ MeV. This corresponds to a rms radius of 0.6 fm for the nucleonic pion source. A very small contribution to q^2 from the *np* mass difference is neglected. For the present purpose, which only concerns the charged pion pole, the pion mass splitting is irrelevant, as well as the charge dependence of the coupling. The amplitudes above have of course the correct normalization at the pion pole.

For the discussion of the qualitative contributions of pion exchange we have chosen for convenience this special form for the pion pole terms. Both the Chew extrapolation procedure and the difference method depend only on the value of the coupling constant at the pole and make no assumption on the particular form of the pion pole terms. In principle this is also the case in the Ashmore approach, but since one wants to decrease the number of expansion parameters, an efficient description of the pion pole terms is desirable. It is of no fundamental importance to any of the methods whether we define the pion Born terms with or without a form factor, whether the δ function is included or not, or whether the pseudoscalar or pseudovector definition for the πNN coupling is used. The only important point is that the residue at the pion pole remains unaffected. However, since the pure pion Born term fails to give a qualitatively correct angular distribution, it is convenient as an orientation to the importance of pion exchange to use these regularized pion Born amplitudes. We have subtracted a constant from the amplitude to ensure a nonzero cross section at 180°, which corresponds to the suppression of the r-space δ function at the

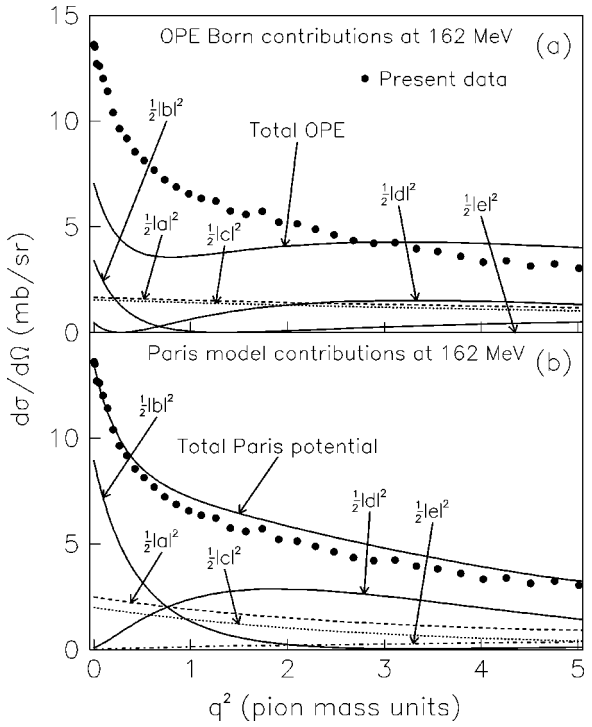

FIG. 11. Illustration of the characteristic contributions to the np differential cross section at 162 MeV using the standard amplitudes a, b, c, d, e according to Eq. (9). (a) the regularized pion Born terms (b) the Paris potential model.

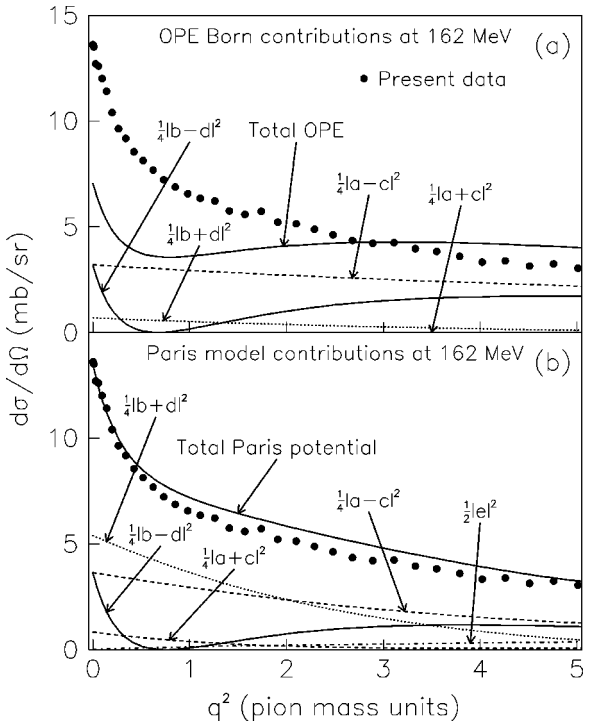

FIG. 12. Same as Fig. 11 for the amplitude combinations of Eq. (13). (a) the regularized pion Born terms (b) the Paris potential model.

origin. This procedure is routinely used since many years in many-body applications of pion physics [46].

The characteristic shape and magnitude of the contributions from the amplitudes a, b, c, d, and e are shown in Figs. 11(a) and 11(b) for the leading order pion exchange and for a realistic model, respectively. We have, somewhat arbitrarily, chosen the Paris model for illustration, but any one of the modern descriptions of the amplitudes would have served the same purpose. According to Eq. (11), where Π_c is the charged pion propagator, the charged pion pole terms contribute only to the amplitudes b and d. To leading order b has contributions from the central, spin-spin, and tensor interactions, while d has pure tensor character [45]. The terms $|a|^2$ and $|c|^2$ give a slowly varying background, while the spin-orbit term $|e|^2$ is negligible. We note that the tensor interaction d, which plays a dominant role in the NN force, vanishes at $q^2=0$, since it requires at least P waves; this term has an important pion component. The amplitude b, which contains the spin-spin interaction term, plays a special role in the extrapolation, since it dominates the physical region in the backward direction closest to the charged pion pole at $q^2=-m_\pi^2$. It is of particular importance to determine this backward region well experimentally, since it is likely to be less constrained by other observables than the region dominated by the tensor amplitude. The extrapolation to the pion pole can also be made using the polarization data for the quantity K_{0nn0} in Eq. (10). It is, however, clear from this equation that this also requires a simultaneous knowledge of the unpolarized differential cross section. Nearly the same precision is required whether one uses polarization data or unpolarized data for the pole extrapolation. For our purpose, there is little or no advantage in the additional complication of polarization experiments, since in both cases we need to know absolute unpolarized or polarized differential cross sections to similar precision, respectively.

Giving up the separation of the amplitudes into terms with obvious physical characteristics it is also interesting to isolate the combination $|b-d|^2$, which contains the entire pion pole term. The corresponding cross section has the following form:

$$\frac{d\sigma}{d\Omega}(q^2)=\frac{1}{2}\left[\frac{1}{2}(|a+c|^2+|a-c|^2)+\frac{1}{2}(|b+d|^2+|b-d|^2)+|e|^2\right], \tag{13}$$

$$\frac{d\sigma}{d\Omega}(q^2)(1-K_{0nn0})=\frac{1}{2}(|b+d|^2+|b-d|^2). \tag{14}$$

The different components for the leading order pion terms defined above, as well as for the more realistic Paris potential, are displayed in Figs. 12(a) and 12(b), respectively. We note that $|b-d|^2$ for the Paris potential, which contains the entire effect of the pion pole, is remarkably close to the Born term, particularly at small q^2. The characteristic zero in the pion Born term for charged pion exchange at $q^2=m_\pi^2/2$ appears here as a deep minimum close to this value. This contribution is thus nearly perturbative and the deep minimum indicates a nearly real amplitude. Similarly, although of much less importance for the understanding of the pole extrapolation, the remaining terms have remarkable features. The term $|a+c|^2$ is very small in both the pion Born term approximation and in the realistic Paris approach and nearly negligible. The term $|a-c|^2$ is more important, but once

more quite close to the Born term. Although less accurate, all the corresponding features are also prominent in the case of antiproton charge exchange. The same pionic features thus show up clearly in both np and $\bar{p}p$ charge exchange reactions [43]. The large modification occurs in the term $|b+d|^2$, which is enhanced by an order of magnitude compared to the Born term, although it is still varying slowly. The corresponding antiproton amplitude appears also strongly modified, but in this case it is nearly totally quenched by annihilation. In conclusion, the contributions from the pionic background terms, consisting of pion form factors and π^0 exchange, have qualitatively a behavior similar to that in a realistic model. The well understood contribution of the pion pole term gives considerable confidence that the extrapolation can be achieved realistically.

B. Extrapolation methods

The basic idea in extrapolating to the pion pole is to first construct a smooth physical function, the Chew function, by multiplying the cross section by $(q^2+m_\pi^2)^2$, which removes the pole term, after which the extrapolation can be made far more safely and controllably. More exactly, we define this function $y(x)$:

$$y(x)=\frac{sx^2}{m_\pi^4 g_R^4}\frac{d\sigma}{d\Omega}(x)=\sum_{i=0}^{n-1} a_i x^i. \tag{15}$$

Here s is the square of the total energy and $x=q^2+m_\pi^2$. At the pion pole $x=0$, the Chew function gives

$$y(0)\equiv a_0\equiv g_{\pi^\pm}^4/g_R^4 \tag{16}$$

in terms of the pseudoscalar coupling constant $g_{\pi^\pm}^2\simeq 14$. The quantity g_R^2 is a reference scale for the coupling chosen for convenience. It is important to realize that the model-independent extrapolation requires accurate data with absolute normalization of the differential cross section. If the differential cross section is incorrectly normalized by a factor N, the extrapolation determines $\sqrt{N}g_{\pi^\pm}^2$. This is one of the most important sources of uncertainty in the practical extrapolation from data.

In the actual analysis the Chew method has been the most common procedure in the past. It expands the Chew function $y(x)$ in terms of a polynomial in q^2. This obviously raises the question of the number of terms which must be included as well as the systematic extrapolation error. The latter point will be examined below. At this point it is valuable to examine how many powers of q^2 are necessary in the Chew polynomial expansion to obtain a plausible extrapolation. One can convince oneself that if the effects of form factors can be neglected and all background terms are constant, then the contributions from the tensor interaction $|d|^2$ will be purely pionic unless at least terms to the third power in q^2 are included and to this order also the leading effect of the πNN form factor is accounted for. Even a minimal account of the shape dependence of the background tensor term requires at least terms to the fourth power in q^2, while the corresponding term in the other amplitudes requires one order less. It is therefore to be expected that the Chew method requires at least five terms in the q^2 expansion.

A second method, which improves the convergence of the Chew method, is the Ashmore method [42]. It parametrizes $d\sigma(x)/d\Omega$ in terms of a pion Born amplitude with an additional background term. In the present context we use the regularized pion Born amplitudes a_π, b_π, c_π, and d_π, given in Eqs. (11) and (12). Since one expects also an important contribution to the np backward scattering from the ρ-meson exchange, we model the Ashmore background amplitude by a pole term simulating ρ exchange with adjustable strength. This expression is fitted to the data and gives in principle a model-independent result for the coupling constant as before. More physics is now built into the procedure, so fewer parameters should be needed. We consider

$$\begin{aligned}\frac{d\sigma}{d\Omega}(q^2)=&\frac{\beta_0}{2g_{\pi^\pm}^4}(a_\pi^2+b_\pi^2+c_\pi^2+d_\pi^2)\\&+\beta_1 P_\rho(q^2)(a_\pi+b_\pi+c_\pi)+\beta_2 P_\rho(q^2)\frac{q^2}{m_\rho^2}d_\pi\\&+P_\rho^2(q^2)\sum_{i=3}^{n-1}\beta_i\left(\frac{q^2}{m_\rho^2}\right)^{i-3},\end{aligned} \tag{17}$$

where the function $P_\rho(q^2)$ is defined as

$$P_\rho(q^2)=\left(\frac{\Lambda_\rho^2-m_\rho^2}{q^2+\Lambda_\rho^2}\right)^2\frac{m_\rho^2}{q^2+m_\rho^2}\frac{1}{\sqrt{s}}. \tag{18}$$

The determination of the coefficient β_0 of the pion Born term gives the coupling constant from data. We apply this model with $\Lambda_\rho=3/2\Lambda_\pi=1200$ MeV and $m_\rho=768.1$ MeV and use it below as an alternative to the Chew method.

The difference method, which we introduced so as to obtain a substantial improvement in the extrapolation procedure [11], is also based on the Chew function, but it recognizes that a major part in the cross section behavior is described by models with exactly known values for the coupling constant. It therefore applies the Chew method to the *difference* between the function $y(x)$ obtained from a model and from the experimental data, i.e.,

$$y_M(x)-y_{\rm exp}(x)=\sum_{i=0}^{n-1} d_i x^i, \tag{19}$$

with g_R of Eq. (15) replaced by the model value g_M. At the pole

$$y_M(0)-y_{\rm exp}(0)\equiv d_0\equiv\frac{g_M^4-g_{\pi^\pm}^4}{g_M^4}. \tag{20}$$

This should diminish systematic extrapolation errors and remove a substantial part of the irrelevant information at large momentum transfers. It is important to realize that we have formally not introduced a model dependence by using such a comparison function and that comparison procedures are

TABLE V. Values of the coupling constant obtained from polynomial fits with n terms to data and ''pseudodata'' at 162 MeV for the reduced range $0<q^2<4\ m_\pi^2$. The experimental values at the minimum $\chi^2/N_{\rm DF}$ are indicated in boldface. The results are given for the Chew method, the Ashmore method, and the difference method. The comparison models are the Nijmegen potential (Nijmegen) and the Nijmegen (NI93) and Virginia (SM95) energy-dependent PWA's. The results are given both for the actual data (Uppsala) as well as for ''pseudodata'' in the models. The model coupling constants are $g^2_{\pi^\pm,\rm Nijmegen}=g^2_{\pi^\pm,\rm NI93}=13.58$, and $g^2_{\pi^\pm,\rm SM95}=13.75$ with $\delta g^2_{\pi^\pm}$ being the systematic shift from the true model value.

n	$\chi^2/N_{\rm DF}$	$g^2_{\pi^\pm}$ Uppsala	$\chi^2/N_{\rm DF}$	$g^2_{\pi^\pm}$ ''Nijmegen''	$\delta g^2_{\pi^\pm}$	$\chi^2/N_{\rm DF}$	$g^2_{\pi^\pm}$ ''NI93''	$\delta g^2_{\pi^\pm}$	$\chi^2/N_{\rm DF}$	$g^2_{\pi^\pm}$ ''SM95''	$\delta g^2_{\pi^\pm}$
					Chew method						
3	7.16	7.14±0.24	7.23	4.95±0.35	8.63	6.55	4.70±0.37	8.88	5.91	5.53±0.31	7.84
4	1.13	12.60±0.36	1.19	11.50±0.39	2.08	1.19	11.12±0.40	2.46	1.13	11.21±0.40	2.54
5	1.07	**13.90±0.82**	1.00	13.38±0.85	0.20	1.00	13.04±0.87	0.54	1.00	13.15±0.87	0.60
6	1.10	14.93±1.93	1.00	13.54±2.20	0.04	1.00	13.40±2.22	0.18	1.00	13.48±2.21	0.27
					Ashmore method						
4	1.03	**14.37±0.46**	1.00	13.43±0.48	0.15	1.01	12.99±0.50	0.59	1.02	12.98±0.50	0.77
5	1.06	14.18±0.97	1.00	13.76±1.01	−0.18	1.00	13.44±1.03	0.14	1.00	13.54±1.02	0.21
					Difference method						
				Nijmegen-Uppsala			NI93-Uppsala			SM95-Uppsala	
1			19.46	13.43±0.02		12.0	13.66±0.02		2.390	14.05±0.02	
2			1.001	14.63±0.05		0.99	**14.58±0.05**		1.079	**14.37±0.05**	
3			0.996	**14.51±0.12**		1.02	14.60±0.12		1.084	14.48±0.12	
4			1.033	14.52±0.31		1.04	14.82±0.30		1.037	14.91±0.30	
5			1.056	14.05±0.81		1.06	14.36±0.79		1.060	14.45±0.79	
				NI93-''SM95''			NI93-''Nijmegen''			SM95-''Nijmegen''	
1			5.70	13.36±0.02	0.39	2.03	13.81±0.02	−0.24	11.1	14.19±0.02	−0.61
2			1.04	13.98±0.05	−0.23	1.07	13.52±0.06	0.06	1.22	13.30±0.06	0.28
3			1.02	13.89±0.12	−0.14	1.02	13.67±0.13	−0.09	1.08	13.54±0.13	0.04
4			1.00	13.66±0.33	0.09	1.00	13.89±0.32	−0.31	1.00	13.98±0.32	−0.40
5			1.00	13.65±0.83	0.10	1.00	13.87±0.82	−0.29	1.00	13.95±0.81	−0.37

used in many contexts of physics to obtain increased transparency and precision. A first step is now to calibrate the method, that is, to establish the precision to which the coupling constant can be determined and the systematic uncertainties that are associated with the extrapolation procedure.

C. Extrapolations to the pion pole

We now investigate these different methods and explore their properties and systematics. For the purpose of determining the systematic uncertainties in the procedures we have generated pseudodata with uncertainties corresponding to the present experiment from 10 000 computer simulations using exact data points from the Nijmegen potential [12] and the Nijmegen energy-dependent PWA NI93 [25] as well as from the Virginia SM95 energy-dependent PWA [18,26] with a Gaussian, random error distribution [47]. The coupling constant was determined for each of these ''experiments'' using the different methods, and its average value for this sample is obtained to high accuracy. We list the result of this exercise in Tables V and VI, where n is the number of terms in the polynomial expansion and $\chi^2/N_{\rm DF}$ is the average χ^2 per degrees of freedom. $g^2_{\pi^\pm}$ is the mean value of the coupling constant for 10 000 pseudoexperiments, while the errors quoted are standard deviations for individual pseudoexperiments. In addition, we also list the systematic deviation $\delta g^2_{\pi^\pm}$ of the mean value in the sample from the true value in the model. We have thus a check on systematic extrapolation errors and can control the corresponding corrections. For the discussion we have grouped the data in two intervals $0<q^2<4\ m_\pi^2$ (''reduced range'' with 31 data points, corresponding to our previous experiment [11]) and $0<q^2<10.1\ m_\pi^2$ (''full range'' with 54 data points). The possibility to group the data in two ranges is very important, as it allows to check the sensitivity and stability of the extrapolation to a particular cut in momentum transfer and to verify that it is the small q^2 region that carries most of the pion pole information. The behavior of $\chi^2/N_{\rm DF}$ as a function of n is characteristic. It falls steeply with increasing n to a value close to unity. Additional terms give only small gains, and the data become rapidly overparametrized. One can then adopt several statistical strategies leading to similar results. One possibility is to extract results at

TABLE VI. Same as for Table V, but for the full range $0<q^2<10.1\ m_\pi^2$.

n	χ^2/N_{DF}	$g^2_{\pi^\pm}$ Uppsala	χ^2/N_{DF}	$g^2_{\pi^\pm}$ "Nijmegen"	$\delta g^2_{\pi^\pm}$	χ^2/N_{DF}	$g^2_{\pi^\pm}$ "NI93"	$\delta g^2_{\pi^\pm}$	χ^2/N_{DF}	$g^2_{\pi^\pm}$ "SM95"	$\delta g^2_{\pi^\pm}$
					Chew method						
5	1.33	12.56±0.28	1.18	11.84±0.30	1.74	1.16	11.48±0.31	2.10	1.15	11.56±0.30	2.19
6	1.17	**13.84±0.48**	1.02	13.10±0.51	0.48	1.02	12.69±0.53	0.99	1.03	12.71±0.53	1.04
7	1.17	14.63±0.83	1.00	13.80±0.87	−0.22	1.00	13.40±0.90	0.18	1.00	13.55±0.88	0.20
					Ashmore method						
4	5.46	11.47±0.34	3.87	11.87±0.34	1.71	4.02	10.92±0.36	2.66	5.54	10.28±0.38	3.47
5	1.15	**14.53±0.33**	1.04	13.99±0.34	−0.41	1.04	13.60±0.35	−0.02	1.05	13.66±0.35	0.09
6	1.17	14.26±0.76	1.03	13.39±0.81	0.19	1.03	12.97±0.83	0.61	1.04	13.02±0.83	0.73
7	1.18	14.48±0.79	1.00	13.71±0.83	−0.13	1.00	13.29±0.86	0.29	1.00	13.41±0.85	0.34
					Difference method						
				Nijmegen-Uppsala			NI93-Uppsala			SM95-Uppsala	
2			3.53	14.34±0.04		2.98	14.31±0.04		1.24	14.28±0.04	
3			1.59	14.97±0.07		1.29	14.91±0.07		1.11	14.47±0.08	
4			1.12	**14.43±0.14**		1.11	**14.55±0.13**		1.10	**14.58±0.13**	
5			1.12	14.20±0.25		1.13	14.50±0.24		1.13	14.61±0.24	
6			1.15	14.29±0.47		1.15	14.65±0.46		1.14	14.80±0.45	
				NI93-"SM95"			NI93-"Nijmegen"			SM95-"Nijmegen"	
2			2.19	13.79±0.05	−0.04	1.08	13.55±0.05	0.03	2.74	13.52±0.05	0.06
3			1.37	14.22±0.08	−0.47	1.07	13.50±0.08	0.08	1.74	13.01±0.09	0.57
4			1.00	13.72±0.14	0.03	1.02	13.70±0.14	−0.12	1.03	13.74±0.14	−0.16
5			1.00	13.64±0.26	0.11	1.00	13.88±0.25	−0.30	1.00	13.99±0.25	−0.41
6			1.00	13.59±0.50	0.16	1.00	13.95±0.48	−0.37	1.00	14.10±0.48	−0.52

the minimum χ^2/N_{DF}. In practice this minimum is a very shallow one, and as a consequence, values of n close to $n([\chi^2/N_{DF}]_{min})$ are nearly equally probable statistically. Another method is to extract $g^2_{\pi^\pm}$ from one of the smallest values of n consistent with a χ^2/N_{DF} well within the range expected from the experimental sample. We remind the reader that in the present case there is about 47% probability of the experimental χ^2/N_{DF} to be larger than unity, and about 25% for it to be larger than 1.15.

For the Chew model a perfect fit is achieved with a fourth order polynomial in q^2 for the reduced range, but with a small systematic downward shift of 0.20 (Nijmegen potential), 0.54 (NI93), and 0.60 (SM95) as compared to the original model values. With a third order polynomial fit the statistical error becomes smaller, but the systematic shift is unacceptably large (2.08, 2.46, and 2.54, respectively). When the full range of data is used, one or two more terms are required to achieve a good fit. In both cases a systematic shift remains even when a perfect fit is achieved, but this shift is always less than the statistical uncertainty. The present experimental data for both ranges give similar results for $g^2_{\pi^\pm}$ at minimum χ^2, but the values are higher than in the models by 0.5 to 1 unit. This points to a higher experimental value for $g^2_{\pi^\pm}$ than in the comparison models. In view of the systematic error of 2 to 4% for the corresponding number of terms in the expansion as well as the large statistical and extrapolation error we will not attempt a precision determination of the coupling constant using this method. The results further substantiate the conclusions of our first report of the present work, where we also used the Paris potential for pseudoexperiments [11].

In the case of the Ashmore method a good description is achieved in the reduced range with one term less in the expansion. This shows that the physics beyond the π exchange is reasonably described by the ρ exchange, as expected. The systematic shifts are similar to those in the Chew model, as seen from Table V. The statistical extrapolation error is reduced, however. The experimental data tend once more to a $g^2_{\pi^\pm}$ that is higher than in the comparison models by about 0.5 to 1 unit. Also in the full range the needed number of terms is smaller (see Table VI). Although there are some improvements in the statistical and extrapolation accuracy, this method also appears to lack the high accuracy we aim at.

The difference method requires only a few terms in the polynomial expansion in favorable cases, and this gives a small, statistical extrapolation error.[2] The similarity between

[2]Recall that the statistical errors have only a meaning when χ^2/N_{DF} is close to 1.

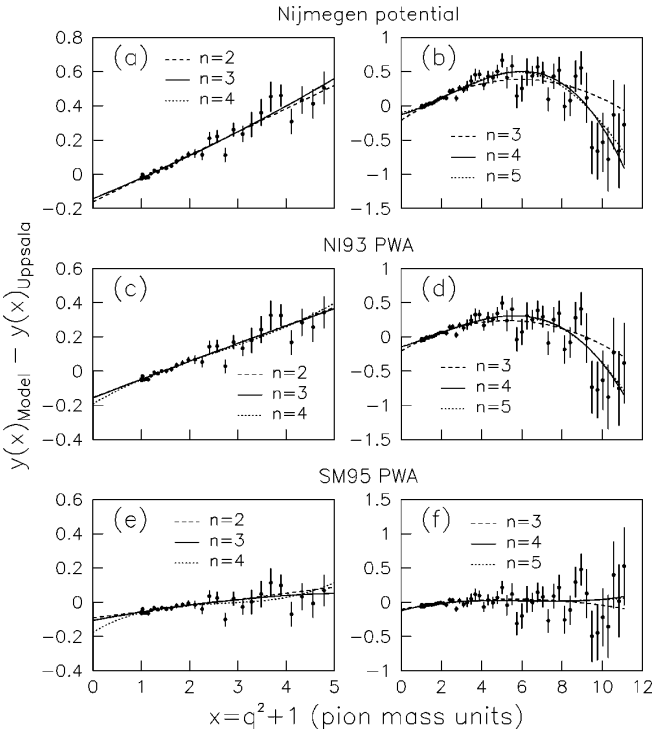

FIG. 13. Extrapolations of the Chew function $y(q^2)$ to the pion pole at 162 MeV with the difference method using different comparison functions, different order of polynomials and different intervals in q^2. The left panel uses the reduced range $0<q^2<4\ m_\pi^2$; the right panel uses the full range $0<q^2<10.1\ m_\pi^2$. The comparison functions are: the Nijmegen potential model (top); the Nijmegen energy-dependent PWA NI93 (middle); and the Virginia energy-dependent PWA SM95 (bottom).

the angular distributions from models and the experimental data is exploited, particularly for large q^2. This incorporates substantial additional physical information without introducing any model dependence. We apply the method using the three comparison models considered above. The result is shown in Fig. 13 for the reduced and full ranges of data. As can be seen, the error bars blow up at large x, which is a consequence of the multiplication of the cross section with x^2, leading to a smaller weight for the large q^2 region in the extrapolation. In all cases the extrapolation to the pole can be made easily and already a visual extrapolation gives a good result. The polynomial fits cause no problem as long as the data are not overparametrized. If this is the case, edge effects in the fitting begin to influence the results [see Fig. 13(e), $n=4$, as an example], but the uncertainty also becomes large. The results are consistent with our previous findings [11]. The data at large q^2 carry little information about the pion. They only serve to stabilize the expansion and remove unstable fits in the lower range.

As a check on the systematic uncertainties in the extrapolation procedure we now examine the results for the pseudodata in detail. We first note that for all the models and all values of n (when $\chi^2/N_{\rm DF}$ approaches 1) there are only a few systematic deviations that are clearly outside the statistical uncertainty. For the SM95-''Nijmegen'' difference it occurs in the full range (Table VI) for $n=3$ with 0.57 and in the reduced range (Table V) for $n=2$ with 0.28. In particular,

TABLE VII. Deviation of $g^2_{\pi^\pm}$ and $\chi^2/N_{\rm DF}$ from the values for NI93-Uppsala of Tables V and VI when an angular distribution that is flatter, but consistent within one standard deviation, is used. The difference method with NI93 as model was employed. The errors are the statistical extrapolation errors as given in Tables V and VI.

	Reduced range		Full range	
n	$\Delta g^2_{\pi^\pm}$	$\Delta\chi^2/N_{\rm DF}$	$\Delta g^2_{\pi^\pm}$	$\Delta\chi^2/N_{\rm DF}$
1	-0.06 ± 0.02	0.08		
2	-0.06 ± 0.05	0.00	-0.09 ± 0.04	0.54
3	-0.01 ± 0.12	-0.01	-0.01 ± 0.07	0.00
4	-0.06 ± 0.30	-0.01	-0.01 ± 0.13	0.00
5	-0.18 ± 0.79	-0.02	-0.03 ± 0.24	0.00
6			-0.12 ± 0.46	0.01

the former case has a poor $\chi^2/N_{\rm DF}$ and the latter one is not good. Since the systematic shift for the NI93-''SM95'' difference follows mathematically by subtracting the NI93-''Nijmegen'' systematic shift from the SM95-''Nijmegen'' one, the same effect will also occur for the NI93-''SM95'' difference, as seen in Tables V and VI. The origin of this systematic shift is apparent in Figs. 13(b) and 13(d), which show the difference Nijmegen-Uppsala and NI93-Uppsala, respectively. The extrapolated values for $n=3$ are 14.97 and 14.91, respectively, both high values and clearly associated with the poor fit to the data. The corresponding difference for SM95 is flat with a good $\chi^2/N_{\rm DF}$, which indicates a considerable similarity in shape to the data. The poor fit will thus also appear for the difference between SM95 and the Nijmegen model for $n=3$. This systematic effect does not influence our analysis, because the minimum in $\chi^2/N_{\rm DF}$ for the Nijmegen-Uppsala difference occurs for $n=4$ in this case and then the systematic shift is small. In the reduced range the shift for the SM95-''Nijmegen'' difference for $n=2$ is only 0.28 (2%) and its exact origin is more difficult to ascertain. It appears associated with the somewhat lower value for the extrapolated coupling constant for the SM95-Uppsala difference for $n=2$ (14.37). This is the largest systematic effect in the present extrapolation procedure, and is of the same order as the normalization uncertainty. While it is already rather small, this systematic shift is largely eliminated by going from $n=2$ to $n=3$.

Finally, the full range of the present experimental data corresponds to five partially overlapping experimental data subsets. We have investigated the uncertainty in $g^2_{\pi^\pm}$ resulting from the small uncertainties in the shape, produced by the matching procedure described in the previous section. We chose a flatter shape of the data by changing the slope by one standard deviation. We extract $g^2_{\pi^\pm}$ using the difference method with NI93. The deviations for $g^2_{\pi^\pm}$ and $\chi^2/N_{\rm DF}$ from the corresponding values in Tables V and VI are given in Table VII. The close agreement is obvious and no substantial error has been added. Similar results are obtained also with the other comparison models. There has been concern that the experimental matching procedure might produce substantial systematic errors (see, e.g., Ref. [48]). The present detailed examination of the situation indicates that this is not the case and that the issue is not a serious one. This conclu-

sion remains also if the errors of the matching coefficients are slightly increased to take the relatively large χ^2 of the first and fourth overlapping regions into account.

For the full range of q^2 we find optimum fits to the experimental data for $n=4$, where the systematic shifts are within 1%. In the reduced range, the optimum fits occur for $n=2$ or $n=3$. The systematic shifts are slightly larger for $n=2$, but going to $n=3$ brings them down to below 1%. The corresponding change in the $g^2_{\pi^\pm}$ determined from the experimental data is negligible. Our conclusion is therefore that the systematic error in our method is at most 2%, and more realistically about 1%. Averaging the values from the extrapolations over the full range we find $\sqrt{N}g^2_{\pi^\pm}=14.52\pm0.13$. The systematic uncertainty is realistically estimated to be ±0.15. The same procedure applied to the interval $0<q^2<4\ m^2_\pi$ gives $\sqrt{N}g^2_{\pi^\pm}=14.49\pm0.07$ with a similar systematic error. In both cases the uncertainty from normalization is 1.2%, i.e., ±0.17. Since the results are nearly identical, this substantiates our statement that the relevant information is nearly entirely at low q^2. In view of the somewhat larger systematic uncertainty in the case of the reduced range, we have adopted the full range value, although this has no practical influence. Therefore, the first value $14.52\pm0.13\pm0.15\pm0.17$ replaces our previously quoted values [11,13].

Our analysis of the present precise experiment on np charge exchange demonstrates that such data can be used for a direct and accurate determination of the πNN coupling constant. We reproduce the original coupling constant using the present procedures for pseudodata from the Nijmegen potential and from the NI93 and SM95 PWA's. The extrapolation error varies considerably, however, and it goes up with the number of parameters. Our value is substantialy larger than the Nijmegen result $g^2_{\pi^\pm}=13.58\pm0.05$, but it is consistent with values given in earlier data compilations based on the analysis of πN and NN scattering data [49].

Subsequent to our first publication [11] Arndt *et al.* [26] subjected a major part of the np charge exchange differential cross section data to an analysis using the difference method. They deduced the coupling constant at many different energies from 0.1 to 1 GeV and found average values between 13.31 and 13.76 depending on the details on the choice of comparison models. This analysis confirms the general statement that the backward np cross sections indeed can be extrapolated to give values for the coupling constant. However, their individual results show a considerable scatter of approximately $\pm10\%$. A large part of this appears to originate from the quality of the data. In particular, the deduced $g^2_{\pi^\pm}$ show obvious systematic and unexpected trends with energy within rather narrow energy intervals. Further, the normalization of most of the data, crucial for conclusions, is subject to considerable caution as we have previously emphasized. In part of the investigation Arndt *et al.* normalize the experimental data to the standard Virginia solution SM95 with $g^2_{\pi^\pm}=13.75$. Finally, their analysis uses rather high powers of polynomials in the fitting procedure. A considerable part of the advantage of the difference method can easily be lost in such a case. As we have seen, the relevant information is concentrated to *small* momentum transfers. It is essential when aiming for high precision to analyze every extrapolation in great detail. One can then make sure that systematic effects of the extrapolation do not influence the conclusions, and that there is complete consistency. Such problems may be particularly dangerous in the case of a large range of momentum transfers.

We found that pseudodata of the same quality as our experiment allows one to reproduce reliably the model coupling constant to about 2% and that a careful inspection of edge effects allowed one to reduce this to 1%. The sensitivity of np charge exchange data to the coupling constant is thus well established. This follows as well from the analysis by the Virginia group, although in this case it is dependent on the quality of the data and shows a larger spread [26]. On the other hand the Nijmegen group concludes within their analysis that $g^2_{\pi^\pm}$ is insensitive to the np backward cross section data [5]. These two findings are in apparent contradiction and it is desirable to understand the origin of the discrepancy. The Nijmegen group has over the last years performed a detailed, global analysis of pp and np scattering data using an energy-dependent PWA. As a by-product of this analysis they extract a value of about 13.6 for $g^2_{\pi^\pm}$, considerably lower than the earlier values [49]. Similar values have later been obtained by the Virginia group as well, also using energy-dependent PWA's [7]. Unfortunately, there exists no independent ''calibration'' of the procedure and the systematic error is unknown. The Nijmegen group has attempted to identify those data which are critical for the determination of $g^2_{\pi^\pm}$ [5]. Their conclusion within their analysis is that $g^2_{\pi^\pm}$ depends diffusely on a number of observables, none being decisive and that the np charge exchange data are nearly irrelevant. We believe that this conflict has its roots, at least partly, in the fact that the Nijmegen group considers the absolute normalization of np cross sections for data sets to be very poorly constrained. Therefore they let the normalization float nearly freely. Since the normalization is crucial for our determination, we suspect that they achieve normalization by indirect means, and that it is implicitly determined via other observables. This would remove the conflict concerning sensitivity.

The normalization of different data sets is a notorious problem when making comparisons. Most data below the pion production threshold at 275 MeV have a floating normalization and will therefore just give the angular shape. Above about 300 MeV, many measurements have been normalized by a simultaneous measurement of the $np\to d\pi^0$ cross section, converting data from the corresponding reaction $pp\to d\pi^+$, and correcting for Coulomb, threshold and isospin effects. Because of the many difficulties involved in this procedure, it is hard to obtain a precision of better than $\pm10\%$ in such a normalization. These and many other data problems will be discussed in some detail in a forthcoming paper [15].

In addition to the lack of sensitivity to the data which for us is essential, the Nijmegen group as with the Virginia group finds a substantially lower value for the coupling constant than we do (see Table VIII). We remind the reader that their analysis is based partly on an important set of data in conflict with the ones we are using here, as discussed previously. The potential impact from this on their conclusion is

TABLE VIII. Recent determinations of πNN coupling constants.

Coupling constant	Source	Reference
$g^2_{\pi^\pm}=14.28\pm0.18$	$\pi^\pm p$ scattering; dispersion relations	Koch and Pietarinen [1]
$g^2_{\pi^0}=14.52\pm0.40$	pp scattering; forward dispersion relations	Kroll [2]
$g^2_{\pi^0}=13.47\pm0.11$	NN scattering; PWA	Stoks *et al.* [5]
$g^2_{\pi^\pm}=13.58\pm0.05$	NN scattering; PWA	Stoks *et al.* [5]
$g^2_{\pi^\pm}=13.75\pm0.15$	$\pi^\pm N$ scattering; GMO sum rule	Arndt *et al.* [8]
$g^2_{\pi^\pm}\simeq13.7$	NN scattering; PWA	Arndt *et al.* [7]
$g^2_{\pi^\pm}=14.52\pm0.26$	np scattering; difference method	Present work

presently not known. Further, 1–2 % is a high precision and the rules of precision physics apply. This raises a question of principle concerning the primary determination of an important physical constant such as $g^2_{\pi^\pm}$, independently of the value that is found. The experimental and theoretical procedures must be as transparent and reproducible as possible, and ideally they should be improvable. It is fundamentally undesirable to compound information from many different sources with different systematic errors. In addition, it would be valuable to have a clear demonstration that the procedure of analysis indeed reproduces the coupling constant from pseudodata to the accuracy that is quoted. This would provide a clear demonstration that no systematical errors of importance have been introduced. Although the determinations by the Nijmegen and the Virginia groups based on energy-dependent PWA analysis are interesting, they cannot definitely settle the issue of the coupling constant.

The charge exchange reaction $\bar{p}p\to\bar{n}n$ has the same charged pion Born terms as for np charge exchange and is therefore in principle a similar source of information on $g^2_{\pi^\pm}$. The recent experimental data are superior in quality to those in np charge exchange both in normalization, in statistics and in the fact that they now cover the entire angular range, at least at one energy [50]. The authors of Refs. [51,52] have used the Chew method to extract $g^2_{\pi^\pm}=12.80$ from these data. We have also recently analyzed these data in detail [43]. Unfortunately, they do not appear to give quite the same precision as the one that can be achieved in the np case. The reasons are the following: first, annihilation causes a strong reduction of the cross section in the region most sensitive to the pion. In addition, the overall knowledge of elastic antiproton reactions is less detailed than for NN reactions. The difference method is then less useful and efficient in the case of antiprotons. One is faced with relying on the Chew method, which is more exposed to systematics. The reaction $\bar{p}p\to\bar{n}n$ gives a low value for $g^2_{\pi^\pm}$ of 13.0 with a formally small statistical error. For the reasons stated, the real systematic error appears to be of the order of 0.7, i.e., 5%. This still makes it interesting in the present discussion, but it is not decisive in the precision determination and in the choice between a high and a low value for the coupling constant.

VI. SUMMARY AND CONCLUSIONS

The np differential cross section has been measured at 162 MeV in the angular range $72°-180°$, using a magnetic proton recoil spectrometer. The data were normalized using the total np cross section, which is one of the most accurately known cross sections in nuclear physics, together with a novel approach, in which the differential cross section measurement was considered as a simultaneous measurement of a fraction of the total cross section. To relate our data to the total cross section as measured by Lisowski *et al.* [19] and Grundies *et al.* [20], this fraction was determined using the angular shape of a number of energy-dependent PWA's. We believe that the normalization obtained in this way is good to within $\pm2.3\%$.

The present data have been compared with other data sets published in the literature. To be able to compare also with data at other energies, the cross sections were displayed as $d\sigma/dt$ versus t. It was found that in the angular region $150°-180°$ our data are steeper than those of the large data set of Bonner *et al.* [16] below about 400 MeV, while they are more similar to the Bonner data at higher energies. The shape agreement between our data and those of Hürster *et al.* [17], which cover the energy range 200–580 MeV, is excellent.

Comparisons have also been performed with several PWA's and NN potential models. Also here it was found that our data are steeper at the backward angles, which is not surprising, since these models were obtained by fitting to the existing data (with the exclusion of those of Hürster). It is interesting to note, however, that the present data are best described in the $72°-150°$ region by the SM95 PWA (Refs. [18,26]), which was obtained by fitting to data up to 1.6 GeV. Thus, it seems as, down to 162 MeV, this PWA brings some of the high-energy information, which, as we have shown, is in better agreement with our data.

The present data have been used to determine a precise value for the charged πNN coupling constant using extrapolation to the pion pole. Using the most accurate extrapolation method, the difference method, we find $\sqrt{N}g^2_{\pi^\pm}=14.52\pm0.13$ ($f^2_{\pi^\pm}=0.0803\pm0.0007$) with a systematic error of about ±0.15 (±0.0008) and a normalization uncertainty of ±0.17 (±0.0009). We have no difficulty in reproducing the input coupling constants of models using equivalent pseudodata. The practical usefulness of the method, its precision and its relative insensitivity to systematics appear to be in hand without serious problems. It is noteworthy that the pseudodata demonstrate that considerable precision is achieved statistically at a single energy. However, the absolute normalization of the data is crucial. The method we use has not yet reached its theoretical limit, but we can now pinpoint the key information necessary for this in the NN sector. We require unpolarized differential cross sections

with an absolute normalization of 1 to 2% to reach a precision of about 1% in the coupling constant. Presently this is achieved using integration over an incomplete angular distribution. It is important to extend the angular range of data, simply to achieve an improved normalization. In principle, a single experiment at one energy is enough to determine $g^2_{\pi^\pm}$, for all energies contain similar, in fact nearly identical, information. Although the method of analysis does not appear in question, it is, however, desirable to deduce the coupling constant from data at several energies. This would increase confidence that no inadvertent systematic effect influences the conclusion.

ACKNOWLEDGMENTS

We thank The Svedberg Laboratory crew for careful operation of the cyclotron. We are also grateful to M. Lacombe for discussions on contributions to the cross sections for the Paris potential, and to W.R. Gibbs for advice on producing pseudodata from models. T.E. acknowledges an interesting discussion with M. Rentmeester and B.L. the hospitality of The Svedberg Laboratory. This work was financially supported by the Swedish Natural Science Research Council and by the CNRS French-Swedish Bilateral Cooperation Program. Unité de Recherche des Universités Paris 11 et Paris 6 Associée au CNRS.

[1] R. Koch and E. Pietarinen, Nucl. Phys. **A336**, 331 (1980).
[2] P. Kroll, *Physics Data*, edited by H. Behrens and G. Ebel (Fachinformationszentrum, Karlsruhe, 1981), Vol. 22-1.
[3] J. R. Bergervoet, P. C. van Campen, R. A. M. Klomp, J.-L. de Kok, T. A. Rijken, V. G. J. Stoks, and J. J. de Swart, Phys. Rev. C **41**, 1435 (1990).
[4] R. A. M. Klomp, V. G. J. Stoks, and J. J. de Swart, Phys. Rev. C **44**, R1258 (1991).
[5] V. Stoks, R. Timmermans, and J. J. de Swart, Phys. Rev. C **47**, 512 (1993).
[6] R. A. Arndt, Z. Li, D. Roper, and R. L. Workman, Phys. Rev. Lett. **65**, 157 (1990).
[7] R. A. Arndt, I. I. Strakovsky, and R. L. Workman, Phys. Rev. C **50**, 2731 (1994).
[8] R. A. Arndt, R. L. Workman, and M. M. Pavan, Phys. Rev. C **49**, 2729 (1994).
[9] T. Meissner and E. M. Henley, Phys. Rev. C **55**, 3093 (1997).
[10] T. E. O. Ericson, Nucl. Phys. **A543**, 409c (1992).
[11] T. E. O. Ericson, B. Loiseau, J. Nilsson, N. Olsson, J. Blomgren, H. Condé, K. Elmgren, O. Jonsson, L. Nilsson, P.-U. Renberg, A. Ringbom, T. Rönnqvist, G. Tibell, and R. Zorro, Phys. Rev. Lett. **75**, 1046 (1995).
[12] V. G. J. Stoks, R. A. M. Klomp, C. P. F. Terheggen, and J. J. de Swart, Phys. Rev. C **49**, 2950 (1994). Data as given by SAID, Ref. [18].
[13] T. E. O. Ericson, B. Loiseau, J. Blomgren, and N. Olsson, πN Newsletter **12**, 16 (1996).
[14] T. Rönnqvist, H. Condé, N. Olsson, R. Zorro, J. Blomgren, G. Tibell, O. Jonsson, L. Nilsson, P.-U. Renberg, and S. Y. van der Werf, Phys. Rev. C **45**, R496 (1992).
[15] J. Blomgren, N. Olsson, and J. Rahm (unpublished).
[16] B. E. Bonner, J. E. Simmons, C. L. Hollas, C. R. Newsom, P. J. Riley, G. Glass, and Mahavir Jain, Phys. Rev. Lett. **41**, 1200 (1978).
[17] W. Hürster, T. Fischer, G. Hammel, K. Kern, M. Kleinschmidt, L. Lehmann, H. Schmitt, L. Schmitt, and D. M. Sheppard, Phys. Lett. **90B**, 367 (1980).
[18] Scattering Analysis Interactive Dial-Up (SAID), Virginia Polytechnic Institute, Blackburg, VA [R. A. Arndt (private communication)].
[19] P. W. Lisowski, R. E. Shamu, G. F. Auchampaugh, N. S. P. King, M. S. Moore, G. L. Morgan, and T. S. Singleton, Phys. Rev. Lett. **49**, 255 (1982).
[20] V. Grundies, J. Franz, E. Rössle, and H. Schmitt, Phys. Lett. **158B**, 15 (1985).
[21] H. Condé, S. Hultqvist, N. Olsson, T. Rönnqvist, R. Zorro, J. Blomgren, G. Tibell, A. Håkansson, O. Jonsson, A. Lindholm, L. Nilsson, P.-U. Renberg, A. Brockstedt, P. Ekström, M. Österlund, F. P. Brady, and Z. Szeflinski, Nucl. Instrum. Methods Phys. Res. A **292**, 121 (1990).
[22] B. Höistad, E. Nilsson, J. Thun, S. Dahlgren, S. Isaksson, G. S. Adams, and H. Ikegami, Nucl. Instrum. Methods Phys. Res. A **295**, 172 (1990).
[23] R. C. Byrd and W. C. Sailor, Nucl. Instrum. Methods Phys. Res. A **264**, 494 (1989).
[24] R. F. Carlson, At. Data Nucl. Data Table **63**, 93 (1996).
[25] V. G. J. Stoks, R. A. M. Klomp, M. C. M. Rentmeester, and J. J. de Swart, Phys. Rev. C **48**, 792 (1993). Data as given by SAID, Ref. [18].
[26] R. A. Arndt, I. I. Strakovsky, and R. L. Workman, Phys. Rev. C **52**, 2246 (1995).
[27] D. F. Measday and J. N. Palmieri, Nucl. Phys. **85**, 142 (1966).
[28] M. Lacombe, B. Loiseau, J. M. Richard, R. Vinh Mau, J. Côté, P. Pirès, and R. de Tourreil, Phys. Rev. C **21**, 861 (1980).
[29] R. Machleidt, K. Holinde, and Ch. Elster, Phys. Rep. **149**, 1 (1987).
[30] D. F. Measday, Phys. Rev. **142**, 584 (1966).
[31] J. N. Palmieri and J. P. Wolfe, Phys. Rev. C **3**, 144 (1971).
[32] G. Breit, A. N. Christakis, M. H. Hull, H. M. Ruppel, and R. E. Seamon, Bull. Am. Phys. Soc. **9**, 378 (1964).
[33] A. J. Bersbach, R. E. Mischke, and T. J. Devlin, Phys. Rev. D **13**, 535 (1976).
[34] R. Wilson, Ann. Phys. (N.Y.) **32**, 193 (1965).
[35] J. Franz, V. Grundies, A. Habib, W. Hürster, G. Nicklas, E. Rössle, G. Rupp, H. Schmitt, L. Schmitt, and H. Woolverton (unpublished).
[36] M. L. Goldberger and S. B. Treiman, Phys. Rev. **110**, 1178 (1958).
[37] K. Schreckenbach, P. Liaud, R. Kossakowski, H. Nastoll, A. Bussiere, and J. P. Guillaud, Phys. Lett. B **349**, 427 (1995).
[38] Particle Data Tables, Phys. Rev. D **54**, 1 (1996). In this paperk $\sqrt{2}f_\pi$ is given as f_π.
[39] J. Gasser, M. Sainio, and A. Švarc, Nucl. Phys. **B307**, 779 (1988).
[40] G. F. Chew, Phys. Rev. **112**, 1380 (1958).
[41] P. Cziffra and M. J. Moravcsik, Phys. Rev. **116**, 226 (1959).
[42] A. Ashmore, W. H. Range, R. T. Taylor, B. M. Townes, L.

Castillejo, and R. F. Peierls, Nucl. Phys. **36**, 258 (1962).
[43] T. E. O. Ericson and B. Loiseau, Phys. Lett. B **393**, 167 (1996).
[44] J. Bystricky, F. Lehar, and P. Winternitz, J. Phys. (France) **39**, 1 (1978).
[45] W. R. Gibbs and B. Loiseau, Phys. Rev. C **50**, 2742 (1994).
[46] T. E. O. Ericson and W. Weise, *Pions and Nuclei* (Clarendon Press, Oxford, 1988).
[47] See, e.g., William R. Gibbs, *Computation in Modern Physics* (World Scientific, Singapore, 1994), p. 35.
[48] M. C. M. Rentmeester and R. G. E. Timmermans, Nucl. Phys. A (to be published).
[49] O. Dumbrajs, R. Koch, H. Pilkuhn, G. C. Oades, H. Behrens, J. J. de Swart, and P. Kroll, Nucl. Phys. **B216**, 277 (1983).
[50] R. Birsa, F. Bradamante, A. Bressan, S. Dalla Torre-Colautti, M. Giorgi, M. Lamanna, A. Martin, A. Penzo, P. Schiavon, F. Tessarotto, A. M. Zanetti, A. De Falco, M. P. Macciotta, A. Masoni, G. Puddu, S. Serci, A. Ahmidouch, E. Heer, R. Hess, C. Mascarini, R. Rapin, J. Arvieux, R. Bertini, J. C. Faivre, R. A. Kunne, and M. Agnello, Phys. Lett. B **339**, 325 (1994); Nucl. Phys. (Proc. Suppl.) **B56**, 27 (1997).
[51] F. Bradamante, A. Bressan, M. Lamanna, and A. Martin, Phys. Lett. B **343**, 431 (1995).
[52] F. Bradamante and A. Martin, Phys. Lett. B **343**, 427 (1995).